

Stronger increases but greater variability in global mangrove productivity compared to that of adjacent terrestrial forests

Received: 15 November 2022

Accepted: 31 October 2023

Published online: 3 January 2024

 Check for updates

Zhen Zhang ^{1,2}, Xiangzhong Luo ^{2,3} , Daniel A. Friess⁴, Songhan Wang⁵, Yi Li¹ & Yangfan Li ¹ 

Mangrove forests are a highly productive ecosystem with important potential to offset anthropogenic greenhouse gas emissions. Mangroves are expected to respond differently to climate change compared to terrestrial forests owing to their location in the tidal environment and unique ecophysiological characteristics, but the magnitude of difference remains uncertain at the global scale. Here we use satellite observations to examine mean trends and interannual variability in the productivity of global mangrove forests and nearby terrestrial evergreen broadleaf forests from 2001 to 2020. Although both types of ecosystem experienced significant recent increases in productivity, mangroves exhibited a stronger increasing trend and greater interannual variability in productivity than evergreen broadleaf forests on three-quarters of their co-occurring coasts. The difference in productivity trends is attributed to the stronger CO₂ fertilization effect on mangrove photosynthesis, while the discrepancy in interannual variability is attributed to the higher sensitivities to variations in precipitation and sea level. Our results indicate that mangroves will have a faster increase in productivity than terrestrial forests in a CO₂-rich future but may suffer more from deficits in water availability, highlighting a key difference between terrestrial and tidal ecosystems in their responses to climate change.

Mangrove forests are an important intertidal ecosystem along the coasts of 121 countries in tropical, subtropical and warm temperate zones¹. As blue carbon ecosystems, they are capable of storing and sequestering large volumes of carbon², providing valuable ecosystem services³ to mitigate climate change impacts. Mangroves sequester carbon at a high average rate⁴ of $168 \pm 36 \text{ gC m}^{-2} \text{ yr}^{-1}$ and are able to store it at high densities⁵, with an average of $1,023 \pm 88 \text{ MgC}$ per hectare in the Indo-Pacific, almost four times more than the carbon sequestration

rates and storage densities of terrestrial tropical forests. However, mangroves are substantially influenced by climatic changes^{2,6,7}. For example, mangrove forests along the northern coast of Australia experienced a pronounced dieback in 2015 due to water scarcity induced by an El Niño-driven drought and extremely low sea levels in conjunction with changing lunar cycles^{8,9}. Climate change impacts on mangroves are expected to increase further in the future if current emissions trajectories are maintained⁶. Therefore, understanding how climate influences

¹State Key Laboratory of Marine Environmental Science, Key Laboratory of Coastal and Wetland Ecosystems (Ministry of Education), College of the Environment and Ecology, Xiamen University, Xiamen, China. ²Department of Geography, National University of Singapore, Singapore, Singapore. ³Center for Nature-Based Climate Solutions, National University of Singapore, Singapore, Singapore. ⁴Department of Earth and Environmental Sciences, Tulane University, New Orleans, LA, USA. ⁵Jiangsu Collaborative Innovation Center for Modern Crop Production/Key Laboratory of Crop Physiology and Ecology in Southern China, Nanjing Agricultural University, Nanjing, China.  e-mail: xzluo.remi@nus.edu.sg; yangf@xmu.edu.cn

the growth and stability of mangroves is an essential prerequisite for conservation and restoration efforts aimed at preserving this critical coastal ecosystem for the future.

Studies using satellite observations and in situ monitoring generally agree that terrestrial vegetation globally is experiencing an overall increasing trend in gross primary productivity (GPP)¹⁰, largely due to elevated atmospheric CO₂ concentration (eCO₂)¹¹ and extended growing seasons induced by warming¹². However, coastal ecosystems may respond differently due to their unique ecophysiology and environmental settings. In comparison to terrestrial forests, mangroves are generally more efficient in water use^{13,14} and have lower light compensation points and higher maximum photosynthesis rates¹⁵. Additionally, mangroves are adapted to intertidal environments characterized by fluctuating inundation, salinity and water availability, all of which are tightly regulated by water inputs from tides and precipitation versus water loss from transpiration. These environmental fluctuations have resulted in specific physiological responses and adaptations in mangrove vegetation^{16,17} and thus different responses in carbon uptake to climatic changes in mangroves compared to terrestrial forests. Although a few studies have noted differences in climatic responses between the two^{15,18,19}, they were conducted at limited sites over short periods and are inadequate to inform our examination of mangrove response to climate over large scales. Current global vegetation models also assume that mangroves share similar productivity sensitivities to those of terrestrial evergreen broadleaf forests^{20–22} and are therefore inadequate to accurately predict the responses of mangrove ecosystems to environmental changes.

To improve our understanding of how mangroves respond differently to climate and environmental changes and the underlying mechanisms, we quantify the long-term trends and interannual variability (IAV) in carbon uptake from 2001 to 2020 for mangroves and their nearby terrestrial counterparts, evergreen broadleaf forests (EBFs; note that mangroves are also evergreen broadleaf woody plants). To do so, we used the near-infrared reflectance of vegetation (NIRv)²³, a remotely sensed proxy for GPP^{24,25} retrieved from 250 m Moderate Resolution Imaging Spectroradiometer (MODIS) surface reflectance data. To avoid the confounding effects of direct anthropogenic disturbance and spectral mixture, we limit our analysis to undisturbed mangrove and EBF areas with high forest coverage (>80%) and no detected land cover changes over the past two decades (Methods). Furthermore, we quantify the contribution of various environmental factors to GPP, including air temperature, precipitation, vapour pressure deficit (VPD, an indicator of atmospheric dryness), wind speed (serving as a proxy for the intensity of tropical cyclones), sea surface height (SSH, to quantify changes in sea level) and atmospheric CO₂ concentration, using a factorial simulation method (see Methods for details), and provide mechanistic explanations to the observed differences in productivity changes between tidal mangroves and terrestrial forests at a global scale.

Results

Greater productivity trend and IAV in mangroves

NIRv has been tested theoretically and empirically as a robust proxy for GPP over global ecosystems, including EBFs²³. To further assess its applicability to mangroves, we compared GPP estimates from three mangrove flux tower sites (Supplementary Table 1) with MODIS-based NIRv and observed statistically significant positive correlations across all sites (Extended Data Fig. 1), suggesting that NIRv is a valid proxy for canopy photosynthesis for mangroves.

We examined the trends in photosynthesis for mangroves and neighbouring EBFs by estimating the slope of NIRv over time (Methods). Globally, both mangroves and EBFs displayed an overall increasing trend (that is, increasing annual NIRv) over the investigated years (Extended Data Fig. 2a). The global average NIRv increased by 0.21% (0.14–0.28%; 95% confidence intervals (CI)) and 0.11% (0.03–0.16%) per

year for mangroves and EBFs, respectively. Overall NIRv trends were significantly positive in tropical/subtropical America ($P < 0.001$) and Asia (mangroves: $P < 0.001$; EBFs: $P = 0.013$), and slightly significant in Oceania for both mangroves ($P = 0.098$) and EBFs ($P = 0.028$) (Extended Data Fig. 2b,d,e). Mangroves and EBFs in Australia experienced a substantial increase in NIRv prior to 2010 (Extended Data Fig. 2e), followed by a plateau that corresponded to changes in precipitation and SSH (Extended Data Fig. 2o). In Africa, there was no significant overall trend ($P = 0.422$) for either mangroves or EBFs, but a substantial increase was observed after 2015 (Extended Data Fig. 2c), coinciding with an increase in precipitation since 2015 (Extended Data Fig. 2m). Grid-scale trend detection showed significant increasing signals ($P < 0.1$) over 38.08% and 26.97% of mangroves and EBFs, respectively (34.03% and 19.43% if the significance level α is set to 0.05), mainly concentrated in Southeast Asia, Western Australia and the Caribbean coasts (Fig. 1a). Moreover, the latitudinal patterns of trend rates indicated an increase in productivity enhancement with latitude in the Northern Hemisphere (Fig. 1a), aligning with previous studies²⁶ that have observed growth enhancement in mangroves at latitudinal range limits.

We also observed significant negative trends in NIRv for 10.50% of mangroves and 4.23% of EBFs (or 7.76% and 2.88% respectively, with α set to 0.05), primarily occurring in Southeast Africa, Amazon regions and northern Australia (for mangroves solely) (Fig. 1a). For example, a 7,400 ha loss of mangroves along a 1,000 km stretch of coastline in the Gulf of Carpentaria⁸ of Australia caused a substantial negative anomaly in NIRv in 2015 (Fig. 1a). These local-scale reductions in NIRv resulted in a relatively small overall trend at the continental scale in Africa and Oceania (Extended Data Fig. 2c,e).

To determine whether mangroves respond differently to climate compared to EBFs, we conducted a paired comparison by analysing grid cells where mangroves and EBFs coexist (Methods). Our analysis revealed that, although both mangroves and EBFs experienced an increasing trend in productivity over time, mangroves exhibited a significantly stronger trend ($P < 0.001$, Wilcoxon signed-rank test). On average, the rate of increase in mangrove productivity was nearly double that of EBFs (0.59% per year versus 0.31% per year; Fig. 2a). This result held true whether we considered only significant paired grid cells (Fig. 2a) or all paired grid cells (including those with nonsignificant observations; Fig. 2b). Additionally, we observed a significant stronger negative trend in mangroves than EBFs ($P = 0.044$ for significant paired grids and $P < 0.001$ for all paired grids), although the difference was less pronounced than the positive trend (Fig. 2a,b). Even for those paired grids with opposite trend direction between mangroves and EBFs, the stronger trends in mangroves persisted (Fig. 2a,b). These differences in trends between mangroves and EBFs remained consistent across various comparison methods (paired versus independent) (Supplementary Fig. 1), sample selections (considering all grids or only significant grids) (Fig. 2a,b) and mangrove extent definitions (including pure pixels or mixed pixels) (Supplementary Fig. 2).

We further assessed the IAV in GPP for both mangroves and EBFs by using the coefficient of variation of detrended NIRv (Methods). Both mangroves and EBFs exhibited apparent interannual variations in their global average detrended NIRv, with the largest negative departure from normal occurring in 2015, coinciding with the most extreme El Niño event within our study period (Fig. 3a). Notably, NIRv IAV was most pronounced in the Gulf of Carpentaria of Australia, the Middle East and the Caribbean coasts for mangroves, as well as along the eastern coast of Australia for EBFs (Fig. 1b). Continental analysis revealed that high IAV was particularly evident in Australia and Asia (Extended Data Fig. 2i,j). We also observed that mangroves and EBFs located at higher latitudes exhibited stronger IAV than those in lower latitudes (Fig. 2b).

The IAV in productivity for mangroves (3.74%, 95% CI: 3.64–3.86%) was significantly higher than that for EBFs (2.65%, 95% CI: 2.59–2.72%), regardless of using paired or independent comparisons

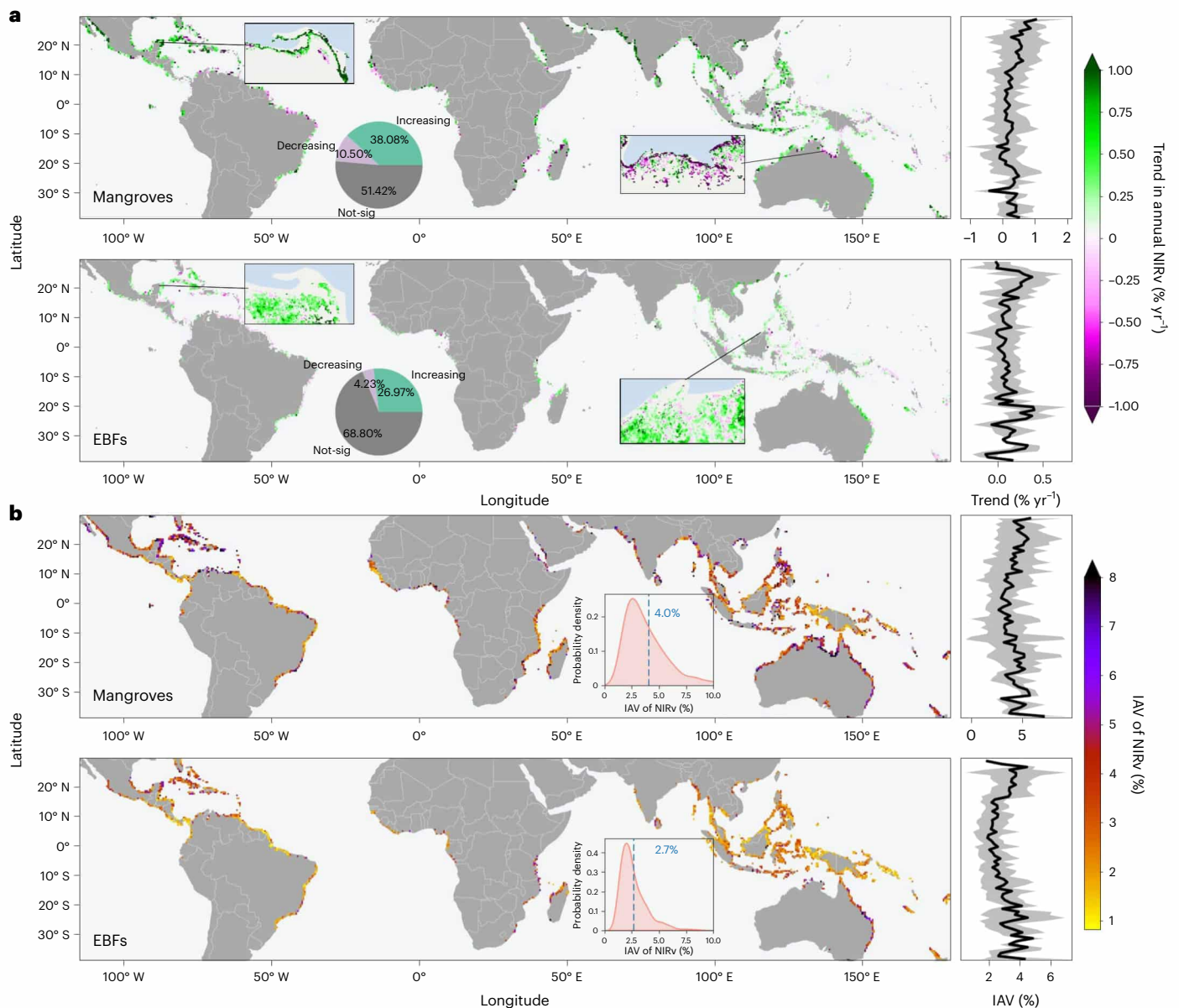


Fig. 1 | Changes in NIRv during 2001–2020 for mangroves and EBFs at the global scale. a, b, Geographic distribution of trends (a) and interannual variability (b) in annual mean NIRv at the $0.5^\circ \times 0.5^\circ$ grid-cell scale. Inset maps in a illustrate exemplary regional trends in NIRv with 250 m resolution. The pie plots indicate the area-weighted proportion of grid cells with increasing productivity, decreasing productivity or nonsignificant ('not-sig') productivity trends ($P > 0.1$).

P values were determined through two-sided Mann–Kendall trend test. The inset plots in b illustrate the probability density curves of IAV with the average indicated by the dashed blue lines and the numbers in blue indicating the global average IAV value. The right-hand panels depict the latitudinal pattern of trends and IAV averaged per 1° latitude band.

(Fig. 2c,d). Taken together, 90.31% of grid cells showed either a stronger trend, a greater IAV, or both, in mangroves than EBFs over the past 20 years (Fig. 2e).

Greater IAV driven by the higher sensitivity to hydroclimate

To gain insight into the relative role of environmental drivers in the IAV in GPP of mangroves and EBFs, we quantified the contribution of five environmental factors (air temperature, VPD, precipitation, wind speed and SSH; Supplementary Table 2) to the NIRv IAV using a model experiment simulation approach (Methods; Supplementary Table 3).

Fluctuation in SSH was the primary driver for IAV in NIRv of mangroves, contributing to 31.67% of satellite-observed IAV in NIRv for mangroves (contributing 1.27% in the total IAV of 4.01%; Fig. 3b). The Gulf of Carpentaria in Australia, where a pronounced negative trend

in NIRv for mangroves was observed (Fig. 1), was found to be dominated by sea level with a co-occurring sea level drop and mangrove dieback event in 2015 (Extended Data Fig. 3). Since the IAV in NIRv for EBFs was not influenced by tide variation (Methods), the observed Δ IAV between mangroves and EBFs was mainly attributed to sea level fluctuation (Fig. 3b).

Meanwhile, our analysis identified precipitation as the dominant climatic factor driving the IAV in NIRv for both mangroves and EBFs. Examination of the global average NIRv and climatic factors (Fig. 3a) revealed a strong positive correlation between NIRv and precipitation ($r = 0.84$ for EBFs and $r = 0.60$ for mangroves), whereas the relationships with temperature, VPD and wind speed were weak or nonsignificant. This finding was further substantiated through factorial simulation, indicating precipitation as the primary climatic factor driving NIRv

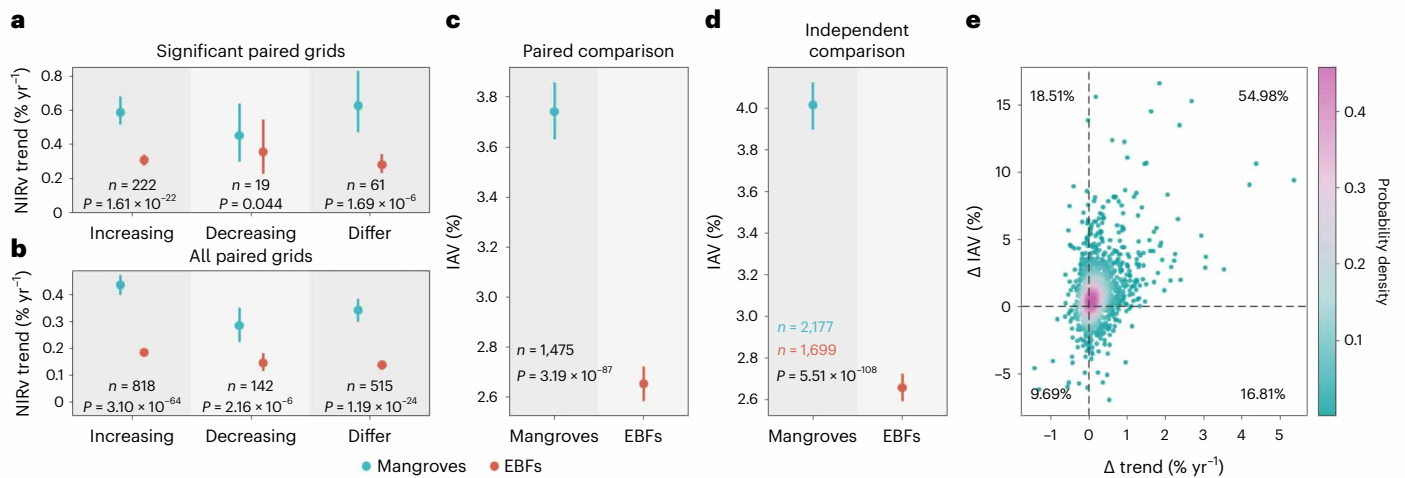


Fig. 2 | Comparisons in NIRv trends and IAV between mangroves and EBFs.

a, b, Differences in NIRv trends between mangroves and EBFs by comparing paired grids with significance (**a**) or all paired grids including nonsignificant grids (**b**), grouped by trend direction. The term ‘differ’ refers to those paired grids with opposite trend direction in mangroves and EBFs. For visualization, we show the absolute value of trend here. *P* values were determined by two-sided

paired *t*-test controlling for geographical locations and macroclimatic factors. **c, d**, Differences in IAV between mangroves and EBFs using two-sided paired *t*-test (**c**) or independent *t*-test analysis (**d**). Error bars in **a–d** show 95% CI estimated by bootstrapping ($n = 1,000$) and the points represent average values. **e**, Relationship between trend and IAV differences. The difference (Δ) is defined as mangroves minus EBFs. Points in the scatterplot refer to the $0.5^\circ \times 0.5^\circ$ grid cells.

IAV (Fig. 3b). Moreover, the impact of precipitation on mangrove NIRv IAV exceeded that on their neighbouring EBFs (Fig. 3b), suggesting a higher sensitivity of mangroves to precipitation changes than EBFs.

Wind speed also played a discernible role in driving greater NIRv IAV for mangroves (Fig. 3b), suggesting that mangrove productivity is more sensitive to tropical cyclones than terrestrial forests. On a global scale, both air temperature and VPD had relatively minor contributions to NIRv IAV for both mangroves and EBFs (Fig. 3b). The use of different climate-forcing datasets did not alter our results regarding the attribution of NIRv IAV (Supplementary Fig. 3). Despite previous reports highlighting the sensitivity of mangroves to cold events²⁷, our global-scale analysis indicated that annual minimum temperature had a lesser influence on NIRv IAV compared to SSH, precipitation and wind speed (Supplementary Fig. 4).

To provide a mechanistic explanation for why mangrove NIRv had higher sensitivity to precipitation, we used a partial differential approach to decompose this sensitivity into two ecohydrological properties: the marginal biological water use fraction ($\partial T_c / \partial P$, which quantifies the change in plant transpiration in response to a unit change in precipitation)²⁸ and the marginal water use efficiency (MWUE, $\partial \text{NIRv} / \partial T_c$, which quantifies the change in GPP in response to a unit change in transpiration) (Methods). We found considerable differences between mangroves and EBFs in these two properties. Specifically, while mangroves generally displayed lower $\partial T_c / \partial P$ than EBFs (Extended Data Fig. 4a), their MWUE ($0.53\% \text{ mm}^{-100}$, 95% CI: $0.16\text{--}0.88\% \text{ mm}^{-100}$) was nearly double that of EBFs ($0.24\% \text{ mm}^{-100}$, 95% CI: $-0.15\text{ to }0.61\% \text{ mm}^{-100}$; Extended Data Fig. 4b), suggesting that the higher sensitivity of mangroves to variations in precipitation is due to their higher efficiency in water use.

Stronger trend caused by greater CO₂ fertilization effect

We further quantified the contributions of temperature, precipitation, VPD, wind speed, SSH and atmospheric CO₂ concentration to the NIRv trend in mangroves and EBFs by using a multivariable linear model during the warming hiatus (2001–2012 in our study period²⁹). We removed the one-year-lagged autocorrelation in NIRv to eliminate the influence of natural vegetation growth, which captures the effects of antecedent vegetation conditions on current ecological processes³⁰. During the warming hiatus, temperature and VPD were stable with no

trends in most regions, yet increasing productivity was still widespread in mangroves and EBFs (Supplementary Fig. 5). This time window provides a unique opportunity³¹ to disentangle the compound effects of warming and eCO₂ on vegetation productivity.

The increasing productivity trends in both mangroves and EBFs were primarily driven by the CO₂ fertilization effect during 2001–2020 (Fig. 4). We estimated the CO₂ fertilization effect to be $0.10\% \text{ ppm}^{-1}$ ($0.09\text{--}0.12\% \text{ ppm}^{-1}$) and $0.05\% \text{ ppm}^{-1}$ ($0.03\text{--}0.06\% \text{ ppm}^{-1}$) for mangroves and EBFs, respectively. During the period of 2001–2020, atmospheric CO₂ concentration increased by 2.20 ppm yr^{-1} based on the NOAA CarbonTracker CT2022 modelling³², resulting in productivity gains of $0.23\% \text{ yr}^{-1}$ ($0.19\text{--}0.27\% \text{ yr}^{-1}$) and $0.10\% \text{ yr}^{-1}$ ($0.07\text{--}0.13\% \text{ yr}^{-1}$) for mangroves and EBFs, respectively (Extended Data Fig. 5). Consequently, the difference in trends observed between mangroves and EBFs during the 2001–2020 period mainly came from the CO₂ fertilization effect.

Warming was diagnosed as the second-largest contributor to global productivity increases in mangroves and EBFs (Fig. 4). However, the contribution of warming to increasing productivity was greater in EBFs than in mangroves, partially offsetting the greater productivity increases in mangroves due to CO₂ fertilization (Fig. 4). The observed minor warming-related global trend in mangroves was due to the offset of positive and negative effects of warming on mangrove productivity over high and low latitudes (Extended Data Fig. 6a), which suggests that warming may suppress mangrove productivity in certain areas, mainly in low-latitude tropical regions (Extended Data Fig. 6a). Increasing VPD had a widespread negative effect on productivity (Extended Data Fig. 6b), offsetting the productivity benefits from warming (Fig. 4). The effects of VPD on productivity were similar for mangroves and EBFs, and therefore VPD contributed little to the satellite-observed trend differences (Fig. 4).

Although precipitation played a dominant role in influencing NIRv IAV, its impact on NIRv trends was limited (Fig. 4). This was primarily due to the lack of a significant long-term trend in precipitation³³ across most of the study areas (Supplementary Fig. 6). In contrast, we identified a significant decline ($\alpha = 0.1$) in annual maximum wind speed in 27.3% of the study area (Supplementary Fig. 6), with a global average decline of 0.014 m s^{-1} per year, which contributed to a slightly positive NIRv trend in mangroves (Fig. 4). Moreover, we detected a modest but positive

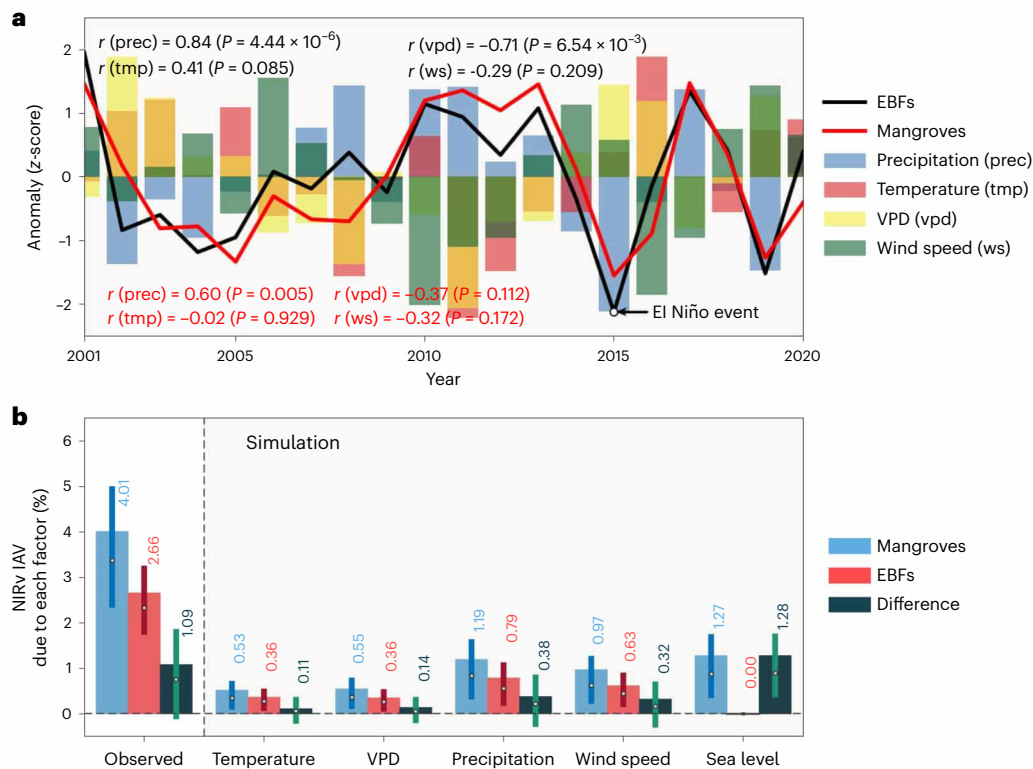


Fig. 3 | Contribution of climatic factors and sea level to NIRv interannual variability. **a**, Time series of detrended global mean NIRv and climatic factors from 2001 to 2020, with all variables normalized to z-score anomaly. The numbers refer to the Pearson correlation. *P* values were determined through two-sided Pearson correlation significance test. Considering the interaction between temperature and VPD, we show their partial correlation coefficient by controlling for the other. **b**, Satellite-observed NIRv IAV and simulated NIRv IAV from each

environmental factor, which was estimated by the product of sensitivity of NIRv to the factor and s.d. of the factor. The bars show the global mean contribution of each factor and the error bars show 95% CI estimated by bootstrapping ($n = 1,000$). All grid cells were used for mangroves and EBFs ($n = 2,177$ and $n = 1,699$, respectively), and for the 'difference' group, paired grid cells ($n = 1,475$) were used, with the difference defined as mangroves minus EBFs. Supplementary Fig. 3 shows an analogous plot using an alternative set of climate data.

effect of sea level rise on non-submerged mangroves (Fig. 4). This effect could potentially be linked to sea level rise alleviating water stress for specific mangrove species situated at relatively high elevations³⁴.

Discussion

Our study reveals a significantly stronger increase and greater interannual variability in GPP for mangroves compared to nearby inland forests over the past 20 years (2001–2020). The greater IAV in mangroves was mainly attributed to their higher sensitivities to fluctuations in sea level and precipitation than EBFs, while the stronger positive trend was attributed to their stronger responses to eCO₂ concentration. Our results highlight the difference between mangroves and EBFs in responding to climate change, emphasizing the need for special characterization of coastal ecosystems such as mangrove forests in global carbon cycle studies.

Over 30% of mangroves and EBFs in this study showed a positive trend in NIRv. Considering that around one-third of global terrestrial vegetation has been observed to be greening using leaf area index since 2000¹² and around 23.6% for global mangroves using the normalized difference vegetation index (NDVI) time series³⁵, we suggest that the increase in NIRv (GPP²³) could be partly interpreted as the increase in leaf area. Meanwhile, the slightly higher percentage reported in this study (34.03% when α was set to 0.05) also means an increase in per-leaf area photosynthesis for mangroves. Previous studies have found NIRv is a stronger indicator of GPP than NDVI for global ecosystems that have C₃ photosynthesis pathways²³, suggesting NIRv serves as a reliable proxy for the GPP of mangroves that also follow the C₃ pathway. We indeed note statistically significant correlations between NIRv and GPP

at three mangrove sites (Extended Data Fig. 1). However, there was one flux site (Everglades) where we found the NIRv–GPP relationship was not strong (although still statistically significant) (Extended Data Fig. 1), probably because the MODIS pixel covering that flux site has a higher percentage of water cover than other sites (Supplementary Fig. 7). In a more homogeneous mangrove pixel, such as the pixel covering Mai Po flux site (Supplementary Fig. 7), NIRv shows a strong correlation with mangrove GPP (Extended Data Fig. 1). Another advantage of NIRv over NDVI lies in its higher signal-to-noise ratio, minimizing signals from non-vegetated backgrounds such as soil and water surfaces under mangrove canopies, which is more suitable for application to mangroves²⁴.

Mangroves exhibited stronger productivity increases in high-latitude subtropical and warm temperate regions than in low-latitude tropical regions. Our simulation on temperature-induced NIRv trend captured a similar latitudinal pattern (Extended Data Fig. 6a), suggesting that the stronger productivity enhancement in the subtropical and warm temperate regions was caused by warming. This finding is consistent with in situ warming experiments^{26,36} and remote sensing studies^{37,38} reporting increased canopy cover and growth in mangroves due to warming, especially near their latitudinal range limits. However, at low latitudes in the Northern Hemisphere, the latitudinal pattern of NIRv trend was better explained by the CO₂ fertilization effect (Extended Data Fig. 5), suggesting that eCO₂ plays a more important role than warming within species thermal limits³⁹. The fertilization effect of eCO₂ on vegetation productivity, especially for C₃ plants, has been well-established in existing research^{40,41}, encompassing experimental studies³⁴, field observations⁴² and global models¹¹. Our estimates of CO₂ fertilization effect for mangroves (0.10% ppm⁻¹)

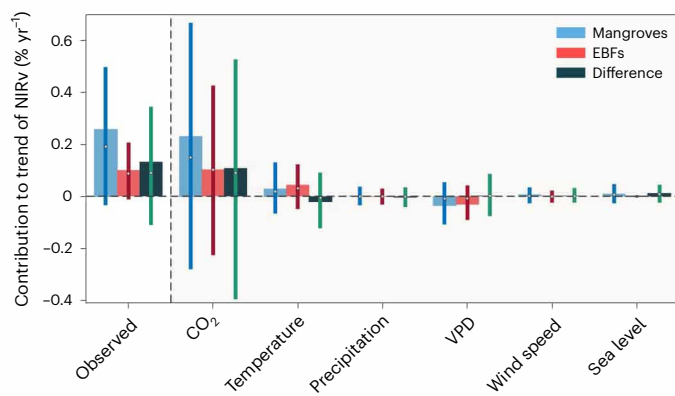


Fig. 4 | Contribution of climatic factors and sea level to NIRv trend. Simulated NIRv trends from each environmental factor, estimated by multiplying the sensitivity of NIRv to the factor and the trend of the factor. Bars show the global mean contribution of each factor and error bars show 95% CI estimated by bootstrapping ($n = 1,000$). For mangroves and EBFs, we used all their grid cells ($n = 2,177$ and $n = 1,699$, respectively); for the group of 'difference', we used paired grid cells ($n = 1,475$), and the difference was defined as mangroves minus EBFs.

and EBFs ($0.05\% \text{ ppm}^{-1}$) are consistent in magnitude with global average estimates of previous process-based ecosystem models ($0.05\text{--}0.20\% \text{ ppm}^{-1}$)⁴³. We found spatial variation in the CO_2 fertilization effect, because increases in photosynthesis with $e\text{CO}_2$ may be constrained by regional limitations in water and nutrient availability⁴⁴ and can vary among different tree species^{40,45}.

The higher MWUE of mangroves (Extended Data Fig. 4b) provides a potential explanation for their greater CO_2 fertilization effect compared to that of EBFs. As atmospheric CO_2 concentration rises, plants reduce their stomatal conductance to maintain a constant ratio of intercellular and atmospheric CO_2 concentration, which decreases transpiration⁴¹ and increases soil water content⁴⁶. The higher MWUE in mangroves amplifies this water-saving effect under elevated CO_2 , resulting in larger increases in productivity⁴⁷. The water saved further alleviates the salinity stress for mangroves to support their growth^{14,40}. Previous theoretical and experimental evidence has demonstrated that water-limited ecosystems generally benefit more in growth and photosynthesis from elevated CO_2 concentrations than non-water-limited ecosystems^{45,48}. Our results are consistent with these findings, as mangroves are more water-limited than the adjacent terrestrial EBFs due to the highly saline tidal environment^{39,49}. We acknowledge that the absolute values of MWUE calculated in this study are subject to uncertainty because we have only three years (2019–2021) of thermal ECOSTRESS observation to quantify transpiration. However, this is plausible for our study because our focus is on a relative comparison between mangroves and EBFs, rather than their absolute values. Ideally, a long-term, high-resolution thermal remote sensing evapotranspiration product would be suitable for this purpose, but it is currently unavailable. The ECOSTRESS evapotranspiration product is estimated based on the energy budget and land surface temperature⁵⁰, which avoids any presumptions on stomatal behaviour and CO_2 impacts. It is also available at a relatively high resolution (70 m), which is compatible with the size of most mangrove forest patches.

While the global average NIRv trend in mangroves was positive, our analysis showed that negative productivity trends in mangroves occurred sporadically across the study area. In particular, we found a larger proportion (10.50%) of areas with negative productivity trends in mangroves than in EBFs, mainly in Madagascar and the northern coast of Australia. These declines in NIRv could be attributed to disturbances from tropical cyclones⁵¹, El Niño-induced droughts and lunar nodal cycle-related sea level anomalies^{9,52}. A specific example in the Gulf of Carpentaria, Australia, showed that negative NIRv trends

observed in mangroves was probably due to dieback events resulting from the compounded effects of extreme low sea level events and precipitation deficits (Extended Data Fig. 3). In addition, increased aquaculture activities can discharge pollutants into the habitats of mangroves, reducing the leaf area of mangroves⁵³ and further leading to a negative NIRv trend. These unique stresses in mangroves, such as sea level fluctuation, aquaculture pollution and stronger disturbance from cyclones, provide an explanation for the observed divergence in the direction of NIRv trends between mangroves and EBFs (Fig. 2a,b).

Mangroves showed stronger IAV in productivity than EBFs, mainly due to their greater sensitivity to precipitation, according to our analysis. There are three possible mechanisms for the higher precipitation sensitivity of mangroves: high-salinity intertidal environments, estuarine hydrology and low diversity of tree species within mangrove ecosystems. First, the high salinity of the tidal seawater reduces the water potential around mangrove roots^{54,55}, imposing greater water limitations on mangroves than on adjacent terrestrial forests⁴⁹. The pseudo-drought (highly saline) tidal environment means that mangroves could be likened to semi-arid ecosystems³⁹, which are well-known for their high sensitivity to water availability⁵⁶ and strong IAV in productivity^{57,58}. In contrast, moist EBFs display high resistance to drought⁵⁹, resulting in more stable productivity over time. As an adaptation to high-salinity intertidal environments, mangroves have evolved a water use efficiency higher than that of most terrestrial C_3 plants^{13,14}, and our investigation provides large-scale evidence for that: mangroves not only have higher water use efficiency (the ratio of GPP to transpiration) but also higher MWUE (changes in GPP with incremental changes in transpiration), which explains the greater benefits from increased precipitation in mangroves over terrestrial forests. Additionally, the lower xylem pressure in mangroves (< -2.5 MPa) than terrestrial forests (-1.6 to -0.5 MPa) due to tidal seawater poses a higher risk of embolism during water deficits¹³. Decreased (increased) precipitation would increase (reduce) sediment porewater salinity through concentrations (dilution) of salts during low tides⁶⁰, reducing (increasing) water uptake by mangrove roots⁵⁴ and further increasing (reducing) the risk of hydraulic failure⁶¹. Furthermore, some mangrove species cope with high salinity through foliar salt secretion and leaf shedding⁶², leading to a decrease in leaf area and NIRv observed by satellites. Second, precipitation variability also regulates estuarine hydrology differently than for EBFs. For example, fluvial discharge brings sediments and nutrients, such as phosphorus and nitrogen, which can influence mangrove growth, particularly in nutrient-limited settings⁶³. Third, mangrove ecosystems are far less diverse than other tropical and subtropical tree communities¹³. Previous research^{64,65} has indicated that ecosystems with limited tree species diversity tend to be more sensitive to water deficits, primarily due to the weaker complementary interactions among species in resisting drought.

Other than precipitation, mangroves also exhibited higher sensitivity to wind speed (Fig. 3b). As mangroves are often distributed at the forefront of tropical cyclone paths and act as a buffer to protect adjacent inland trees⁶⁶, they reduced wind impacts on nearby EBFs. We also observed that sea level fluctuation contributed the most to the stronger IAV of mangrove productivity, consistent with previous studies⁹. Extremely low sea levels can increase soil salinization by 20–30% (ref. 67) and induce physiological water deficit in mangroves. Meanwhile, shifting from anaerobic to aerobic conditions during low tidal levels can lead to phosphorus limitation in mangroves and thus decreased photosynthesis¹³. Considering that we have masked out mangrove observations submerged by tides using a NDVI threshold (Methods), the detected impact of sea level fluctuation mainly reflects the actual adjustments of mangrove productivity to water level changes, rather than an artefact in satellite signal resulting from water inundation. We acknowledge that the water surface under the mangrove canopies might affect the satellite signals on tidal vegetation activity; however, this issue should be minimized by using NIRv, a

vegetation index insensitive to underlying water surfaces and proven to be suitable for monitoring wetland ecosystems such as mangroves²⁴.

In summary, our study examined the dynamics in mangrove productivity over the past 20 years and their response to climate change by comparing with nearby inland forests (that is, EBFs) using satellite observations. We discovered that mangroves exhibit more increases and interannual variability in productivity than EBFs due to greater CO₂ fertilization effects and higher sensitivity to precipitation, sea level fluctuation and wind. These disparities emphasize the need for an explicit inclusion of coastal ecosystems in large-scale vegetation models such as dynamic global vegetation models, which currently ignore such unique coastal processes and characteristics^{20,22}, to improve future projections of climate change impacts across the land–sea interface. Conservation efforts for mangroves may yield a greater carbon gain compared to inland forests due to their higher CO₂ fertilization effects but require special attention to damages caused by extremely low precipitation and low sea level events. Overall, our study highlights the key ecophysiological difference between terrestrial and coastal ecosystems on the global scale and offers a new perspective on coastal forest conservation and restoration under future climate change.

Methods

Generating annual NIRv time series

MODIS instruments on board the Terra and Aqua platforms record the land surface reflectance (SR) at daily revisit frequency for the whole globe and provide 250 m resolution measurements for near-infrared (NIR) and red bands. This presents a better opportunity for monitoring cloud-prone coastal vegetation ecosystems such as mangroves compared to finer but temporally less frequent satellite datasets (for example, Landsat and Sentinel-2 products), which have numerous data gaps in low-latitude areas and are therefore not suitable for our study. We used the Collection 6 Terra and Aqua MODIS 16-day composite SR products (MOD13Q1 and MYD13Q1) at a 250 m resolution from 2001 to 2020 to retrieve the annual NIRv. We excluded observations that were identified as clouds, cloud shadows, snow or aerosols, or that had a high view zenith angle (>30°), by checking the quality flag band to ensure that only high-quality observations were analysed. Considering that tidal inundation could cover mangrove canopies and result in abnormally low NIRv, we removed MODIS observations with NDVI less than 0.2 for each mangrove pixel to eliminate the satellite artefact caused by water inundation on low-lying mangroves⁶⁸. This step filtered out 1.60% (62,674) of 250 m mangrove pixels. To test the feasibility of the NDVI threshold, we examined the NDVI distribution in a region dominated by dwarf mangroves—the Red Sea coasts. Even in this extremely arid region, 96.4% of mangroves have an NDVI greater than 0.2 (Supplementary Fig. 8c), indicating that this threshold is appropriate for capturing dwarf mangroves. Additionally, we tested the trend result from different NDVI thresholds and found that the NIRv trends were consistent with different NDVI thresholds in the tidal filtering step (Supplementary Fig. 8a,b). This suggests that differences in NDVI threshold were unlikely to affect our results. The two SR products (Terra and Aqua) were then merged into a monthly composite by taking the temporal average of all valid observations within the corresponding month. For those months without valid MODIS observations, we gap-filled in their monthly climatology (that is, long-term average) of SR during 2001–2020. Years with no valid observations for more than six months were replaced by the yearly climatology of SR. Finally, we calculated the annual SR by averaging all the derived monthly values within a year and used this annual time-series data in the following analysis.

NIRv, the product of NDVI and NIR reflectance, is a measure of the fraction of the NIR reflected from vegetation and has a stronger correlation with GPP across various vegetation biomes, including terrestrial evergreen forests, compared to other conventional vegetation indices^{23,69,70}. As NIRv minimizes signals from non-vegetated backgrounds, such as water surface under the mangrove canopies²⁴, its variation

mainly reflects the actual variations in mangrove productivity rather than sub-pixel water dynamics. We examined the NIRv–GPP relationship for mangrove forests by comparing MODIS-derived NIRv with GPP measured from mangrove flux sites. Specifically, we systematically reviewed the peer-reviewed publications between 2002 and 2023 reporting mangrove flux data using a Web of Science keyword search with the following terms: TOPIC: (mangrove AND Flux AND (GPP OR NEE)). This returned 24 related studies, of which three mangrove flux data are publicly available, located in the Everglades National Park in the United States⁷¹, Yunxiao in Mainland China^{60,72} and Mai Po in Hong Kong⁷³ (Supplementary Table 1). These sites provide half-hour GPP or net ecosystem exchange, and the latter was partitioned into GPP and ecosystem respiration following ref. 74. Both the half-hour GPP from flux measurements around the MODIS overpass time (that is, 10:30 for Terra and 13:30 for Aqua) and valid 16-day interval MODIS NIRv were aggregated into monthly averages for comparison. We believe that the NIRv–GPP relationship tested in these sites can be considered robust, given their large geographical span and the fact that the relationship has already been validated in other evergreen broadleaf vegetations²³ (as noted, mangroves are also evergreen broadleaf plants).

Gridded climate datasets

We obtained annual mean air temperature (°C), annual mean VPD (kPa) and annual maximum wind speed (m s⁻¹) data from the Modern-Era Retrospective analysis for Research and Applications v.2 (MERRA-2) products⁷⁵ for climate analysis. MERRA-2 provides monthly climate reanalysis data at a 0.5° × 0.625° resolution since 1980 (Supplementary Table 2) with full coverage of both terrestrial and marine areas. VPD is defined as the difference between saturation vapour pressure and actual vapour pressure, and was calculated using the mean air temperature and dew point temperature from MERRA-2 following the equation⁷⁶:

$$\text{VPD} = 0.611 \times e^{\frac{17.27 \times T_a}{237.3 + T_a}} - 0.611 \times e^{\frac{17.27 \times T_d}{237.3 + T_d}} \quad (1)$$

where T_a represents the average daily temperature (°C) and T_d is the dew point temperature.

Annual precipitation data were obtained from Global Precipitation Climatology Project (GPCP)⁷⁷ v.3.2 monthly products with 0.5° × 0.5° resolution, defined as the annual sum of monthly precipitation. It is important to note that in our study the term ‘precipitation’ specifically refers to rainfall, as mangroves are not present in regions with large amounts of snowfall⁷⁸. For sea level fluctuation and rise, we used time-series SSH data from the Copernicus Marine Environment Monitoring Service satellite altimetry measurements with 0.25° × 0.25° resolution (Supplementary Table 2). This data provides SSH as sea level anomaly (m), which is defined as the water level over the long-term mean sea surface from 1993 to 2012. To fill in data gaps in the nearshore area where SSH pixels are missing, we used a 3 × 3 window with the bilinear approach to extrapolate the data from ocean to land⁷⁹. For our analysis of atmospheric CO₂ concentration, we used the gridded data provided by the NOAA CarbonTracker³² CT2022 surface fluxes simulation with a 3° × 2° resolution.

As a robustness check, we conducted a sensitivity analysis using an alternative set of climate data, including ERA5 monthly mean air temperature at 2 m height and VPD with 0.25° resolution⁸⁰, CHIRPS v.2.0 annual precipitation data with 0.05° resolution⁸¹ and TerraClimate⁸² annual maximum wind speed data with 4 km resolution. In addition, we replaced the gridded atmospheric CO₂ concentration data with CO₂ observation data from Mauna Loa Observatory⁸³. Using the ERA5 daily mean air temperature data, we also calculated the length of the growing season for each year, defined as the number of days with a daily average temperature exceeding or equal to 10 °C (ref. 84). However, we observed that almost all of the study areas had a year-long growing season and exhibited minimal interannual variability (Supplementary Fig. 9). We thus excluded the length of the growing season in the subsequent

attribution analysis. All datasets analysed in this study were resampled to a common 0.5° grid using the bilinear method to ensure the same spatial extent of all factors.

Identifying undisturbed areas in mangroves and EBFs

To ensure that NIRv variations arose from dynamics in vegetation productivity rather than in mangrove distribution due to land cover change or sea level rise, we restricted our study area to undisturbed mangrove or EBF pixels. Undisturbed pixels were defined as those that did not exhibit any detectable land cover changes during 2001–2020 and contained at least 80% coverage of the corresponding forest type, following established protocols in related studies^{74,85}. This approach enabled us to exclude any noise signals arising from mixed pixels. Specifically, we first determined an initial undisturbed mangrove extent by extracting consistent mangrove area throughout the study period using the latest mangrove layer, Global Mangrove Watch (GMW) v.3.0 (ref. 1). This consistent part is viewed as the areas with no land cover change during the study period. The mangrove coverage was then calculated as the percentage of the 30 m undisturbed mangrove area within each 250 m MODIS pixel. To determine the initial geographic distribution of undisturbed EBFs, we extracted stable EBF pixels (that is, those with no land cover change) from the MODIS Collection 6 MCD12Q1 International Geosphere–Biosphere Programme (IGBP) yearly land cover product from 2001 to 2020⁸⁶. We then further calculated the percentage of the 30 m global forest change map from ref. 87 within each 250 m EBF pixel to determine the EBF coverage. Note that the EBF layer in the MCD12Q1 IGBP classification maps does not contain mangrove forests, which are instead classified as ‘permanent wetlands’. In cases of geographic overlap, the mangrove layer has priority because of its higher original spatial resolution.

The above steps yielded 3,863,151 mangrove (after tidal filtering) and 11,997,074 EBF pixels at 250 m resolution, respectively. Among these, 1,388,324 (35.94%) and 11,744,704 (97.90%) of mangrove and EBF pixels were identified as pure pixels (coverage >80%) for subsequent analysis. Given a large proportion of mangroves are mixed pixels and were excluded from our main analysis, we also examined the NIRv trend using all 250 m mangroves pixels (with no tidal filtering and including mixed pixels). Including all mangrove pixels resulted in a greater positive trend than using only pure mangrove pixels (Supplementary Fig. 2), which further supports our conclusion that mangroves exhibited stronger productivity enhancement than EBFs. Given the uncertainty associated with the trend derived from mixed pixels, we focus on pure pixels in our main analysis.

Our study area was restricted to 0.5° × 0.5° climate grid cells containing the 250 m undisturbed mangrove pixels; EBFs contained in these grid cells were considered to be the nearby terrestrial counterpart of mangrove forests, as they share the same macroclimatic conditions. The 250 m MODIS NIRv data were then masked by the undisturbed mangrove and EBF layers to obtain their NIRv, which were further aggregated into the 0.5° coastal grid cells by the spatial average to match the gridded climate data.

ECOSTRESS transpiration data

We obtained ECOSTRESS Level 3 Evapotranspiration scenes (ECO3ETPTJPL v.1)⁵⁰ between January 2019 and December 2021 for our study area. This data product has a 70 m spatial resolution and a one-to-five-day temporal interval. It provides daily information on evapotranspiration and the fraction of canopy evaporation. We used this product to get the canopy transpiration (T_c) and aggregated all available scenes within a year into average daily T_c . The annual total T_c was then obtained by multiplying the average daily T_c by 365 days. We resampled the T_c data to 250 m resolution using the bilinear interpolation method and removed pixels that were not detected as mangroves or EBFs. The T_c of mangroves and EBFs were further aggregated to the 0.5° coastal grid cells by their spatial average.

Estimating trends and IAV

We assessed the temporal trends in annual mean NIRv of EBFs and mangroves separately for each coastal grid cell using the Theil–Sen slope estimators and Mann–Kendall trend test method for the period 2001–2020. For better comparisons between mangroves and EBFs, we normalized the trend (that is, grid-level Theil–Sen slope) by the 20-year mean NIRv for each grid cell, expressed as % yr⁻¹. Normalization helped to remove the spatial variations in average NIRv and ensure that observed differences across space were primarily caused by varying responses to environmental changes over time⁸⁸. The significance level α was set as 0.1, consistent with prior studies on vegetation trends^{85,89–91}, to indicate statistically significant increasing (positive Theil–Sen slope) or decreasing (negative Theil–Sen slope) productivity.

The IAV was expressed by the coefficient of variation (CV) of time-series annual NIRv for EBFs and mangroves separately at grid level, calculated as:

$$CV = \frac{\sigma}{\mu} \quad (2)$$

where σ represents the s.d. of linearly detrended time-series NIRv during 2001–2020 and μ is the mean value of time-series NIRv. The detrended s.d. could make us isolate the effect of the annual trend on IAV calculation.

To investigate whether mangroves and EBFs differ in their NIRv trends, we conducted a paired t -test analysis on grid cells with significant NIRv trends for both mangroves and EBFs. The Wilcoxon signed-rank test method, the nonparametric version of the paired t -test, was used if data did not meet the assumptions of normality. With this paired comparison, we eliminate the differences between EBFs and mangroves due to geographic mismatch and focus on the climate impacts. Our results, therefore, can be interpreted as how productivity changes in mangrove and terrestrial EBFs differ under the same climate change conditions. We also performed a robustness check by comparing all grid cells, including those that were not statistically significant, and repeated the same analyses using independent t -test comparison on significant and all grid cells, respectively.

Attribution of interannual variability in productivity through factorial simulation

For each grid cell, we investigated the contributions of climate-system parameters (air temperature, VPD, precipitation and wind speed) and SSH to the IAV of NIRv in mangroves and EBFs. We did not include the interannual variability of atmospheric CO₂ concentration in our IAV attribution as the atmospheric CO₂ concentration exhibited minimal interannual variability (the s.d. of detrended CO₂ concentration is only 0.708–0.854 ppm; Supplementary Fig. 10). In the attribution analysis, we used a factorial simulation approach to construct multivariable linear models, with the detrended NIRv serving as the response variable⁹². Specifically, we first established a normal model (S_{normal}) incorporating all observed independent variables for each grid cell:

$$\text{NIRv} = \gamma_0 + \gamma_T \times T + \gamma_{\text{VPD}} \times \text{VPD} + \gamma_P \times \text{Prec} + \gamma_{\text{WS}} \times \text{Wind} + \gamma_{\text{SSH}} \times \text{SSH} + \varepsilon \quad (3)$$

where γ_0 is the intercept, γ_T , γ_{VPD} , γ_P , γ_{WS} and γ_{SSH} represent the slope of each corresponding independent variable and ε is the model residual; T , VPD, Prec, Wind and SSH correspond to the detrended time-series values of the annual mean air temperature, annual mean VPD, annual total precipitation, annual maximum wind speed and annual mean SSH obtained from gridded climate datasets. Although some terrestrial forests, such as low-lying coastal freshwater forests, can be influenced by saltwater intrusion⁹³, we found that the EBFs we examined were almost free from the impacts of sea level variability, as only 0.05% of the EBFs are within 2 m of sea level (Supplementary Fig. 11), which is

a criterion for determining whether coastal vegetation is influenced by sea level changes⁸⁴. As a result, we set γ_{SSH} to 0 when performing model simulation for EBFs. The partial regression slope of each independent variable normalized by the mean annual NIRv was referred to as climatic sensitivities. The units of climatic sensitivity are, therefore, the proportion of change in annual NIRv per unit of change in each climatic factor. However, since VPD is derived from temperature according to equation (1), the γ_T and γ_{VPD} in S_{normal} cannot be directly interpreted as isolated temperature or VPD sensitivity. We thus ran two additional models (S_T and S_{VPD}) holding T and VPD constant (in the first year—that is, 2001), respectively, and the other four variables to vary with time. The temperature and VPD sensitivities were then estimated from the following equations:

$$\Delta \text{NIRv}_{(S_{normal}-S_T)} = \gamma_0 + \gamma_T \times \Delta T_{(S_{normal}-S_T)} + \varepsilon \quad (4)$$

$$\Delta \text{NIRv}_{(S_{normal}-S_{VPD})} = \gamma_0 + \gamma_{VPD} \times \Delta \text{VPD}_{(S_{normal}-S_{VPD})} + \varepsilon \quad (5)$$

where $\Delta \text{NIRv}_{(S_{normal}-S_{VPD})}$, $\Delta T_{(S_{normal}-S_T)}$ and $\Delta \text{VPD}_{(S_{normal}-S_{VPD})}$ represent the differences in simulated NIRv, observed mean temperature and VPD between models; γ_0 is the intercept and ε is the residual term; and γ_T and γ_{VPD} are isolated sensitivities of NIRv to temperature and VPD variation. The contribution of each factor on NIRv IAV was then quantified as the product of s.d. of each factor and the magnitude of NIRv sensitivity to that factor determined from equations (3–5). Note that the CV is a positive value for vegetation, so we used the absolute value of the sensitivity in quantifying the contribution of each factor to NIRv IAV. The simulated ΔIAV (mangroves minus EBFs) accounted for a substantial portion of satellite-observed difference in IAV ($R^2 = 0.55$ and 0.61 for two environmental forcing datasets; Extended Data Fig. 7a,c).

Attribution of trend in productivity

We included long-term atmospheric CO_2 concentration in trend attribution to account for CO_2 fertilization on vegetation. To disentangle the compound effects of air temperature and CO_2 concentration on observed NIRv trends, we performed a multivariable linear regression analysis during the warming hiatus (before 2013 in our study period)⁹⁴, where atmospheric CO_2 concentration continued to rise but global temperature remained stable. To remove the contribution of the antecedent vegetation conditions to the increase in current NIRv³⁰, we used a first-order autoregression model to estimate the slope of the lag-1 NIRv term against the time series of NIRv and then subtracted the product of the slope and lag-1 NIRv term from raw NIRv time series⁹⁵. The NIRv trend was then attributed to each factor in the following equation with temperature, VPD, precipitation and SSH as control variables:

$$\text{NIRv} = \beta_0 + \beta_T \times T + \beta_{VPD} \times \text{VPD} + \beta_P \times \text{Prec} + \beta_{SSH} \times \text{SSH} + \beta_{\text{CO}_2} \times \text{CO}_2 + \varepsilon \quad (6)$$

where T , VPD, Prec, SSH and CO_2 represent the raw time series of air temperature, VPD, precipitation, SSH and atmospheric CO_2 concentration during warming hiatus; β_0 is the intercept; β_T , β_{VPD} , β_P and β_{SSH} represent the slope of each corresponding control variable; β_{CO_2} is the CO_2 fertilization effect; and ε is the model residual term. β_{SSH} was still set to 0 for EBFs. The isolated effects of temperature and VPD on NIRv trend were quantified using the same approach as in attributing NIRv IAV. The contribution of each factor on NIRv trend was then quantified by multiplying the trend of each factor during 2001–2020 and the corresponding sensitivity of NIRv to that factor. Wind speed was not included in this trend attribution model to increase the degree of freedom in the model, considering that wind disturbance often poses short-term impacts on mangroves and EBFs. However, we still quantified their potential impacts on NIRv trend by multiplying γ_{WS} from equation (3) and the trend of annual maximum wind speed. We also

tested the contribution of wind speed to NIRv trend by incorporating it into equation (6) and found a similar result (Supplementary Fig. 12).

Estimating MWUE

The responses of vegetation to variations in precipitation and CO_2 concentration are both related to their strategy in water use. Therefore, to understand the reason behind the different values of γ_P and β_{CO_2} for mangroves, we calculated the MWUE, the ratio of the marginal increase in carbon gain to the marginal increase in water loss, using a partial derivative approach⁹⁶. Due to the strong correlation between vegetation transpiration and precipitation, γ_P can be expressed as⁵⁶:

$$\gamma_P = \frac{\partial \text{NIRv}}{\partial P} = \frac{\partial \text{NIRv}}{\partial T_c} \times \frac{\partial T_c}{\partial P} \quad (7)$$

where $\frac{\partial \text{NIRv}}{\partial T_c}$ is the proportional change in NIRv with transpiration variation, and $\frac{\partial T_c}{\partial P}$ is the proportional change in transpiration with precipitation, called the marginal biological water use fraction by ref. 28. $\frac{\partial \text{NIRv}}{\partial T_c}$ is roughly equal to $\frac{\partial \text{GPP}}{\partial T_c}$ (that is, MWUE) due to the strong positive correlation between NIRv and GPP. Since the transpiration data provided by ECOSTRESS is only available from July 2018, we estimate the $\frac{\partial T_c}{\partial P}$ using the slope of linear regression model with T_c as response variable and precipitation as independent variable from 2019 to 2021. The MWUE then could be calculated by substituting from equation (7) as follows:

$$\text{MWUE} = \frac{\partial \text{GPP}}{\partial T_c} \approx \frac{\partial \text{NIRv}}{\partial T_c} = \gamma_P / \frac{\partial T_c}{\partial P} \quad (8)$$

We retrieved all these terms for mangroves and EBFs, respectively, for each 0.5° coastal grid cell, and compared them between mangroves and EBFs to gain a mechanistic explanation on observed differences in precipitation sensitivity.

Reporting summary

Further information on research design is available in the Nature Portfolio Reporting Summary linked to this article.

Data availability

All data used in this study are publicly available. The MODIS 250 m spectral reflectance data (MOD13Q1 and MYD13Q1) are available at https://developers.google.com/earth-engine/datasets/catalog/MODIS_006_MOD13Q1 and https://developers.google.com/earth-engine/datasets/catalog/MODIS_006_MYD13Q1. Gridded climate data used in this study are available in Supplementary Table 2. Forest cover data can be found at the following websites: Global Mangrove Watch v.3.0 (<https://zenodo.org/record/6894273>), MCD12Q1 land cover product (https://developers.google.com/earth-engine/datasets/catalog/MODIS_006_MCD12Q1) and global forest change map (https://developers.google.com/earth-engine/datasets/catalog/UMD_hansen_global_forest_change_2021_v1_9). ECOSTRESS evapotranspiration data can be accessed at <https://www.jpl.nasa.gov/missions/ecosystem-spaceborne-thermal-radiometer-experiment-on-space-station-ecostress>. Atmospheric CO_2 concentration recorded by the Mauna Loa Observatory can be accessed at <https://gml.noaa.gov/ccgg/trends/data.html>. The GPP measurements in the three mangrove sites are available in Supplementary Table 1.

Code availability

The code used to analyse these data and generate the results presented in this study can be obtained from <https://github.com/GIS-ZhangZhen/MangroveGreenness>.

References

- Bunting, P. et al. Global mangrove extent change 1996–2020: Global Mangrove Watch version 3.0. *Remote Sens.* **14**, 3657 (2022).
- Lovelock, C. E. & Reef, R. Variable impacts of climate change on blue carbon. *One Earth* **3**, 195–211 (2020).
- Lee, S. Y. et al. Ecological role and services of tropical mangrove ecosystems: a reassessment. *Glob. Ecol. Biogeogr.* **23**, 726–743 (2014).
- Taillardat, P., Friess, D. A. & Lupascu, M. Mangrove blue carbon strategies for climate change mitigation are most effective at the national scale. *Biol. Lett.* **14**, 20180251 (2018).
- Donato, D. C. et al. Mangroves among the most carbon-rich forests in the tropics. *Nat. Geosci.* **4**, 293–297 (2011).
- Friess, D. A., Adame, M. F., Adams, J. B. & Lovelock, C. E. Mangrove forests under climate change in a 2 °C world. *Wiley Interdiscip. Rev. Clim. Change* **13**, e792 (2022).
- Dahdouh-Guebas, F. et al. Cross-cutting research themes for future mangrove forest research. *Nat. Plants* **8**, 1131–1135 (2022).
- Duke, N. C. et al. Large-scale dieback of mangroves in Australia. *Mar. Freshw. Res.* **68**, 1816 (2017).
- Saintilan, N. et al. The lunar nodal cycle controls mangrove canopy cover on the Australian continent. *Sci. Adv.* **8**, eabo6602 (2022).
- Ruehr, S. et al. Evidence and attribution of the enhanced land carbon sink. *Nat. Rev. Earth Environ.* **4**, 518–534 (2023).
- Chen, C., Riley, W. J., Prentice, I. C. & Keenan, T. F. CO₂ fertilization of terrestrial photosynthesis inferred from site to global scales. *Proc. Natl Acad. Sci. USA* **119**, e2115627119 (2022).
- Piao, S. et al. Characteristics, drivers and feedbacks of global greening. *Nat. Rev. Earth Environ.* **1**, 14–27 (2020).
- Ball, M. C. in *Tropical Forest Plant Ecophysiology* (eds Mulkey, S. S. et al.) 461–496 (Springer, 1996).
- Lovelock, C. E., Krauss, K. W., Osland, M. J., Reef, R. & Ball, M. C. in *Tropical Tree Physiology* Vol. 6 (eds Goldstein, G. & Santiago, L.) 149–179 (Springer, 2016).
- Cui, X. et al. Stronger ecosystem carbon sequestration potential of mangrove wetlands with respect to terrestrial forests in subtropical China. *Agric. For. Meteorol.* **249**, 71–80 (2018).
- Naskar, S. & Palit, P. K. Anatomical and physiological adaptations of mangroves. *Wetl. Ecol. Manag.* **23**, 357–370 (2015).
- Srikanth, S., Lum, S. K. Y. & Chen, Z. Mangrove root: adaptations and ecological importance. *Trees* **30**, 451–465 (2016).
- Liang, J. et al. Evapotranspiration characteristics distinct to mangrove ecosystems are revealed by multiple-site observations and a modified two-source model. *Water Resour. Res.* **55**, 11250–11273 (2019).
- Sperry, J. S., Tyree, M. T. & Donnelly, J. R. Vulnerability of xylem to embolism in a mangrove vs an inland species of *Rhizophoraceae*. *Physiol. Plant.* **74**, 276–283 (1988).
- Kumar, D. & Scheiter, S. Biome diversity in South Asia—how can we improve vegetation models to understand global change impact at regional level? *Sci. Total Environ.* **671**, 1001–1016 (2019).
- Ward, N. D. et al. Representing the function and sensitivity of coastal interfaces in Earth system models. *Nat. Commun.* **11**, 2458 (2020).
- LaFond-Hudson, S. & Sulman, B. Modeling strategies and data needs for representing coastal wetland vegetation in land surface models. *New Phytol.* **238**, 938–951 (2023).
- Badgley, G., Field, C. B. & Berry, J. A. Canopy near-infrared reflectance and terrestrial photosynthesis. *Sci. Adv.* **3**, e1602244 (2017).
- Zeng, Y. et al. Optical vegetation indices for monitoring terrestrial ecosystems globally. *Nat. Rev. Earth Environ.* **3**, 477–493 (2022).
- Wang, S. et al. Recent global decline of CO₂ fertilization effects on vegetation photosynthesis. *Science* **370**, 1295–1300 (2020).
- Saintilan, N., Wilson, N. C., Rogers, K., Rajkaran, A. & Krauss, K. W. Mangrove expansion and salt marsh decline at mangrove poleward limits. *Glob. Change Biol.* **20**, 147–157 (2014).
- Cavanaugh, K. C. et al. Climate-driven regime shifts in a mangrove–salt marsh ecotone over the past 250 years. *Proc. Natl Acad. Sci. USA* **116**, 21602–21608 (2019).
- Good, S. P., Moore, G. W. & Miralles, D. G. A mesic maximum in biological water use demarcates biome sensitivity to aridity shifts. *Nat. Ecol. Evol.* **1**, 1883–1888 (2017).
- Modak, A. & Mauritsen, T. The 2000–2012 global warming hiatus more likely with a low climate sensitivity. *Geophys. Res. Lett.* **48**, e2020GL091779 (2021).
- Ogle, K. et al. Quantifying ecological memory in plant and ecosystem processes. *Ecol. Lett.* **18**, 221–235 (2015).
- Ballantyne, A. et al. Accelerating net terrestrial carbon uptake during the warming hiatus due to reduced respiration. *Nat. Clim. Change* **7**, 148–152 (2017).
- Peters, W. et al. An atmospheric perspective on North American carbon dioxide exchange: CarbonTracker. *Proc. Natl Acad. Sci. USA* **104**, 18925–18930 (2007).
- Adler, R. F., Gu, G., Sapiano, M., Wang, J.-J. & Huffman, G. J. Global precipitation: means, variations and trends during the satellite era (1979–2014). *Surv. Geophys.* **38**, 679–699 (2017).
- Jacotot, A., Marchand, C., Gensous, S. & Allenbach, M. Effects of elevated atmospheric CO₂ and increased tidal flooding on leaf gas-exchange parameters of two common mangrove species: *Avicennia marina* and *Rhizophora stylosa*. *Photosynth. Res.* **138**, 249–260 (2018).
- Ruan, L., Yan, M., Zhang, L., Fan, X. & Yang, H. Spatial-temporal NDVI pattern of global mangroves: a growing trend during 2000–2018. *Sci. Total Environ.* **844**, 157075 (2022).
- Chapman, S. K. et al. Mangrove growth response to experimental warming is greatest near the range limit in northeast Florida. *Ecology* **102**, e03320 (2021).
- Cavanaugh, K. C. et al. Sensitivity of mangrove range limits to climate variability. *Glob. Ecol. Biogeogr.* **27**, 925–935 (2018).
- Yao, Q. et al. Mangrove expansion at poleward range limits in North and South America: Late-Holocene climate variability or anthropocene global warming? *Catena* **216**, 106413 (2022).
- Saintilan, N. & Rogers, K. Woody plant encroachment of grasslands: a comparison of terrestrial and wetland settings. *New Phytol.* **205**, 1062–1070 (2015).
- Gu, X. et al. Changes in mangrove blue carbon under elevated atmospheric CO₂. *Ecosyst. Health Sustain.* **9**, 0033 (2023).
- Ainsworth, E. A. & Rogers, A. The response of photosynthesis and stomatal conductance to rising [CO₂]: mechanisms and environmental interactions. *Plant Cell Environ.* **30**, 258–270 (2007).
- Ainsworth, E. A. & Long, S. P. What have we learned from 15 years of free-air CO₂ enrichment (FACE)? A meta-analytic review of the responses of photosynthesis, canopy properties and plant production to rising CO₂. *New Phytol.* **165**, 351–372 (2005).
- Piao, S. et al. Evaluation of terrestrial carbon cycle models for their response to climate variability and to CO₂ trends. *Glob. Change Biol.* **19**, 2117–2132 (2013).
- Terrer, C., Vicca, S., Hungate, B. A., Phillips, R. P. & Prentice, I. C. Mycorrhizal association as a primary control of the CO₂ fertilization effect. *Science* **353**, 72–74 (2016).
- Pan, Y. et al. Contrasting responses of woody and grassland ecosystems to increased CO₂ as water supply varies. *Nat. Ecol. Evol.* **6**, 315–323 (2022).
- Drake, B. G., González-Meler, M. A. & Long, S. P. More efficient plants: a consequence of rising atmospheric CO₂? *Annu. Rev. Plant Physiol. Plant Mol. Biol.* **48**, 609–639 (1997).
- Krauss, K. W. et al. Mangroves provide blue carbon ecological value at a low freshwater cost. *Sci. Rep.* **12**, 17636 (2022).

48. Maschler, J. et al. Links across ecological scales: plant biomass responses to elevated CO₂. *Glob. Change Biol.* **28**, 6115–6134 (2022).
49. Hayes, M. A. et al. Foliar water uptake by coastal wetland plants: a novel water acquisition mechanism in arid and humid subtropical mangroves. *J. Ecol.* **108**, 2625–2637 (2020).
50. Fisher, J. B. et al. ECOSTRESS: NASA's next generation mission to measure evapotranspiration from the International Space Station. *Water Resour. Res.* **56**, e2019WR026058 (2020).
51. Lagomasino, D. et al. Storm surge and ponding explain mangrove dieback in southwest Florida following Hurricane Irma. *Nat. Commun.* **12**, 4003 (2021).
52. Abhik, S. et al. Influence of the 2015–2016 El Niño on the record-breaking mangrove dieback along northern Australia coast. *Sci. Rep.* **11**, 20411 (2021).
53. Yim, M. W. & Tam, N. F. Y. Effects of wastewater-borne heavy metals on mangrove plants and soil microbial activities. *Mar. Pollut. Bull.* **39**, 8 (1999).
54. Passioura, J. B., Ball, M. C. & Knight, J. H. Mangroves may salinize the soil and in so doing limit their transpiration rate. *Funct. Ecol.* **6**, 476 (1992).
55. Ball, M. C. Ecophysiology of mangroves. *Trees* **2**, 129–142 (1988).
56. Zhang, Y. et al. Increasing sensitivity of dryland vegetation greenness to precipitation due to rising atmospheric CO₂. *Nat. Commun.* **13**, 4875 (2022).
57. Ahlström, A. et al. The dominant role of semi-arid ecosystems in the trend and variability of the land CO₂ sink. *Science* **348**, 895–899 (2015).
58. Poulter, B. et al. Contribution of semi-arid ecosystems to interannual variability of the global carbon cycle. *Nature* **509**, 600–603 (2014).
59. Huang, K. & Xia, J. High ecosystem stability of evergreen broadleaf forests under severe droughts. *Glob. Change Biol.* **25**, 3494–3503 (2019).
60. Zhu, X., Sun, C. & Qin, Z. Drought-induced salinity enhancement weakens mangrove greenhouse gas cycling. *J. Geophys. Res. Biogeosci.* **126**, e2021JG006416 (2021).
61. Méndez-Alonzo, R., López-Portillo, J., Moctezuma, C., Bartlett, M. K. & Sack, L. Osmotic and hydraulic adjustment of mangrove saplings to extreme salinity. *Tree Physiol.* **36**, 1562–1572 (2016).
62. Hoppe-Speer, S. C. L., Adams, J. B., Rajkaran, A. & Bailey, D. The response of the red mangrove *Rhizophora mucronata* Lam. to salinity and inundation in South Africa. *Aquat. Bot.* **95**, 71–76 (2011).
63. Reef, R., Feller, I. C. & Lovelock, C. E. Nutrition of mangroves. *Tree Physiol.* **30**, 1148–1160 (2010).
64. Anderegg, W. R. L. et al. Hydraulic diversity of forests regulates ecosystem resilience during drought. *Nature* **561**, 538–541 (2018).
65. Liu, D., Wang, T., Peñuelas, J. & Piao, S. Drought resistance enhanced by tree species diversity in global forests. *Nat. Geosci.* **15**, 800–804 (2022).
66. Hochard, J. P., Hamilton, S. & Barbier, E. B. Mangroves shelter coastal economic activity from cyclones. *Proc. Natl. Acad. Sci. USA* **116**, 12232–12237 (2019).
67. Lovelock, C. E., Feller, I. C., Reef, R., Hickey, S. & Ball, M. C. Mangrove dieback during fluctuating sea levels. *Sci. Rep.* **7**, 1680 (2017).
68. Wang, X. et al. Rebound in China's coastal wetlands following conservation and restoration. *Nat. Sustain.* **4**, 1076–1083 (2021).
69. Mengistu, A. G. et al. Sun-induced fluorescence and near-infrared reflectance of vegetation track the seasonal dynamics of gross primary production over Africa. *Biogeosciences* **18**, 2843–2857 (2021).
70. Zhang, J. et al. NIRv and SIF better estimate phenology than NDVI and EVI: effects of spring and autumn phenology on ecosystem production of planted forests. *Agric. For. Meteorol.* **315**, 108819 (2022).
71. Barr, J. G. et al. Controls on mangrove forest–atmosphere carbon dioxide exchanges in western Everglades National Park. *J. Geophys. Res. Biogeosci.* **115**, G02020 (2010).
72. Zhu, X. et al. Potential of sun-induced chlorophyll fluorescence for indicating mangrove canopy photosynthesis. *J. Geophys. Res. Biogeosci.* **126**, e2020JG006159 (2021).
73. Liu, J., Valach, A., Baldocchi, D. & Lai, D. Y. F. Biophysical controls of ecosystem-scale methane fluxes from a subtropical estuarine mangrove: multiscale, nonlinearity, asynchrony and causality. *Glob. Biogeochem. Cycles* **36**, e2021GB007179 (2022).
74. Feagin, R. A. et al. Tidal wetland gross primary production across the continental United States, 2000–2019. *Glob. Biogeochem. Cycles* **34**, e2019GB006349 (2020).
75. Rienecker, M. M. et al. MERRA: NASA's Modern-Era Retrospective Analysis for Research and Applications. *J. Clim.* **24**, 3624–3648 (2011).
76. Du, J. et al. Global satellite retrievals of the near-surface atmospheric vapor pressure deficit from AMSR-E and AMSR2. *Remote Sens.* **10**, 1175 (2018).
77. Huffman, G. J. et al. The Global Precipitation Climatology Project (GPCP) combined precipitation dataset. *Bull. Am. Meteorol. Soc.* **78**, 5–20 (1997).
78. Osland, M. J. et al. Climatic controls on the global distribution, abundance, and species richness of mangrove forests. *Ecol. Monogr.* **87**, 341–359 (2017).
79. Rovai, A. S. et al. Macroecological patterns of forest structure and allometric scaling in mangrove forests. *Glob. Ecol. Biogeogr.* **30**, 1000–1013 (2021).
80. Hersbach, H. et al. The ERA5 global reanalysis. *Q. J. R. Meteorol. Soc.* **146**, 1999–2049 (2020).
81. Funk, C. et al. The climate hazards infrared precipitation with stations—a new environmental record for monitoring extremes. *Sci. Data* **2**, 150066 (2015).
82. Abatzoglou, J. T., Dobrowski, S. Z., Parks, S. A. & Hegewisch, K. C. TerraClimate, a high-resolution global dataset of monthly climate and climatic water balance from 1958–2015. *Sci. Data* **5**, 170191 (2018).
83. Keeling, C. D. et al. Atmospheric carbon dioxide variations at Mauna Loa Observatory, Hawaii. *Tellus* **28**, 538–551 (1976).
84. Chen, Y. & Kirwan, M. L. Climate-driven decoupling of wetland and upland biomass trends on the mid-Atlantic coast. *Nat. Geosci.* **15**, 913–918 (2022).
85. Zhou, L. et al. Widespread decline of Congo rainforest greenness in the past decade. *Nature* **509**, 86–90 (2014).
86. Sulla-Menashe, D., Gray, J. M., Abercrombie, S. P. & Friedl, M. A. Hierarchical mapping of annual global land cover 2001 to present: the MODIS Collection 6 Land Cover product. *Remote Sens. Environ.* **222**, 183–194 (2019).
87. Hansen, M. C. et al. High-resolution global maps of 21st-century forest cover change. *Science* **342**, 850–853 (2013).
88. Berner, L. T. et al. Summer warming explains widespread but not uniform greening in the Arctic tundra biome. *Nat. Commun.* **11**, 4621 (2020).
89. Chen, C. et al. China and India lead in greening of the world through land-use management. *Nat. Sustain.* **2**, 122–129 (2019).
90. Winkler, A. J. et al. Slowdown of the greening trend in natural vegetation with further rise in atmospheric CO₂. *Biogeosciences* **18**, 4985–5010 (2021).
91. Cortés, J. et al. Where are global vegetation greening and browning trends significant? *Geophys. Res. Lett.* **48**, e2020GL091496 (2021).
92. Yuan, W. et al. Increased atmospheric vapor pressure deficit reduces global vegetation growth. *Sci. Adv.* **5**, eaax1396 (2019).
93. Kirwan, M. L. & Gedan, K. B. Sea-level driven land conversion and the formation of ghost forests. *Nat. Clim. Change* **9**, 450–457 (2019).

94. Medhaug, I., Stolpe, M. B., Fischer, E. M. & Knutti, R. Reconciling controversies about the 'global warming hiatus'. *Nature* **545**, 41–47 (2017).
95. Seddon, A. W. R., Macias-Fauria, M., Long, P. R., Benz, D. & Willis, K. J. Sensitivity of global terrestrial ecosystems to climate variability. *Nature* **531**, 229–232 (2016).
96. Perri, S., Katul, G. G. & Molini, A. Xylem–phloem hydraulic coupling explains multiple osmoregulatory responses to salt stress. *New Phytol.* **224**, 644–662 (2019).

Acknowledgements

Yangfan Li is the main corresponding author of the study. Yangfan Li and Z.Z. acknowledge support from the National Natural Science Foundation of China (Grant No. 42276232), the Internal Program of State Key Laboratory of Marine Environmental Science (Grant No. MELRI2205) and the China Scholarship Council (Grant No. 202106310079). X.L. acknowledges support from the Singapore Ministry of Education (Grant No. A-0003625-00-00) and the Singapore Energy Center core project (Grant No. A-8000179-00-00). D.A.F. thanks Michael and Mathilda Cochran for endowing the Cochran Family Professorship in Earth and Environmental Sciences at Tulane University. We thank N. Xu at Hohai University for his feedback on an earlier version of this work.

Author contributions

Z.Z. conceptualized the study. Z.Z., X.L. and Yangfan Li designed the research. Z.Z. performed the analysis and drafted the initial manuscript. X.L. substantially revised the paper. D.A.F., S.W., Yi Li and Yangfan Li contributed to result interpretation and made substantial contributions to manuscript refinement.

Competing interests

The authors declare no competing interests.

Additional information

Extended data is available for this paper at <https://doi.org/10.1038/s41559-023-02264-w>.

Supplementary information The online version contains supplementary material available at <https://doi.org/10.1038/s41559-023-02264-w>.

Correspondence and requests for materials should be addressed to Xiangzhong Luo or Yangfan Li.

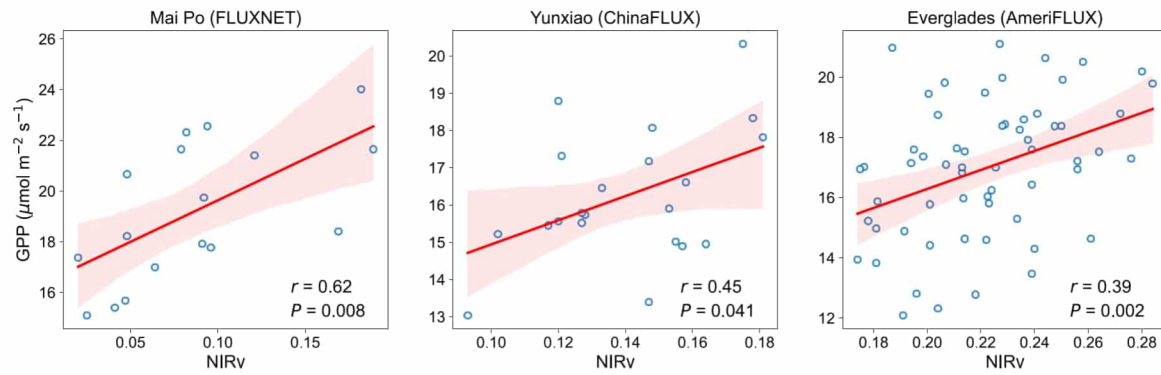
Peer review information *Nature Ecology & Evolution* thanks Lola Fatoyinbo and the other, anonymous, reviewer(s) for their contribution to the peer review of this work. Peer reviewer reports are available.

Reprints and permissions information is available at www.nature.com/reprints.

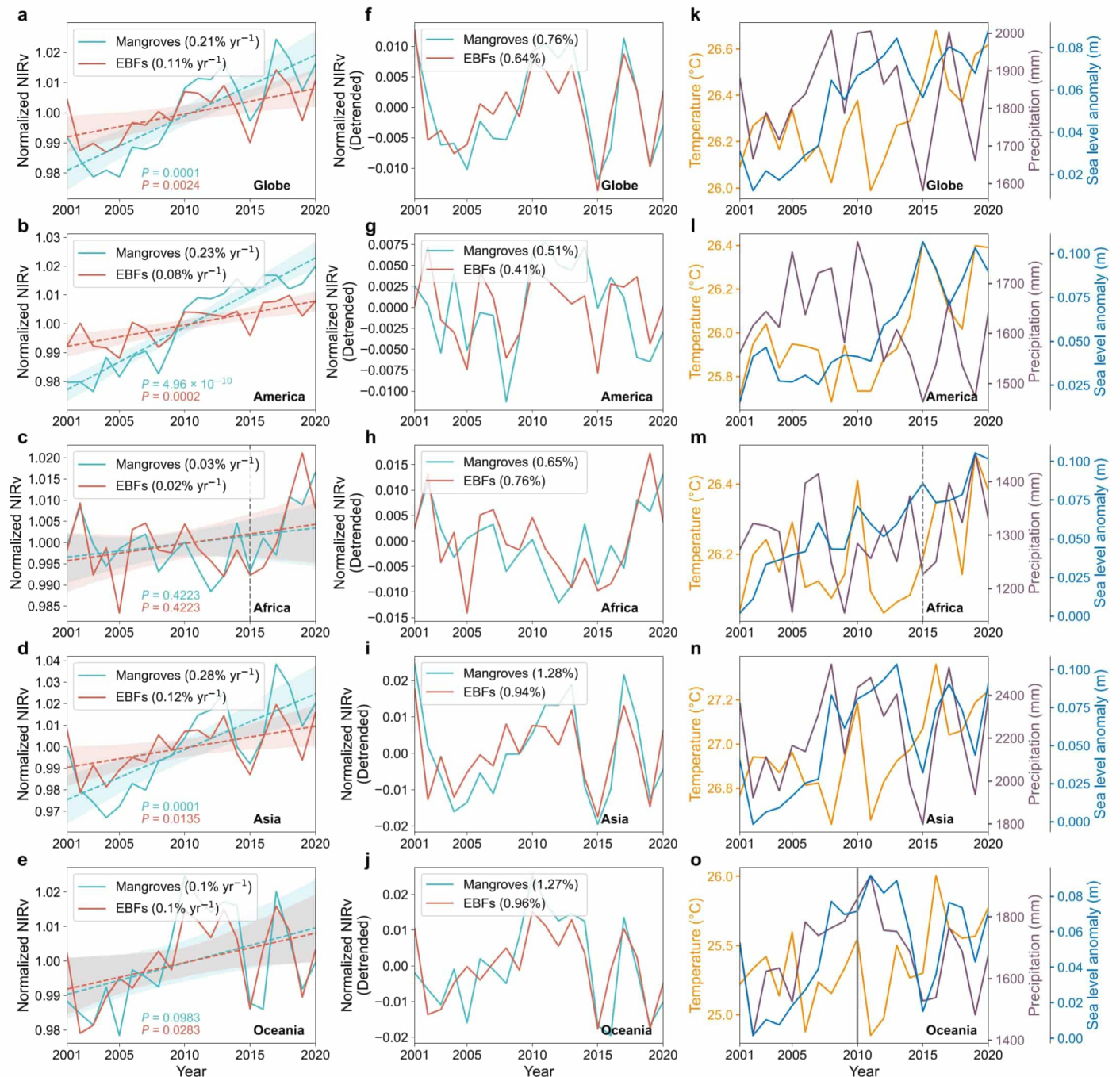
Publisher's note Springer Nature remains neutral with regard to jurisdictional claims in published maps and institutional affiliations.

Springer Nature or its licensor (e.g. a society or other partner) holds exclusive rights to this article under a publishing agreement with the author(s) or other rightsholder(s); author self-archiving of the accepted manuscript version of this article is solely governed by the terms of such publishing agreement and applicable law.

© The Author(s), under exclusive licence to Springer Nature Limited 2024

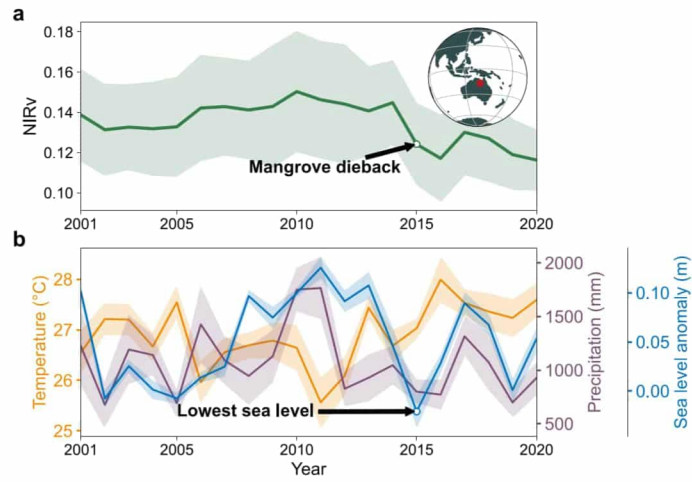


Extended Data Fig. 1 | The correlation between NIRv and GPP at three mangrove flux sites. The red lines give the fitted mean linear relationship between NIRv and GPP. Shading indicates the 95% confidence intervals estimated by bootstrapping ($n = 1000$). P values were determined through two-sided Pearson's correlation significance test.

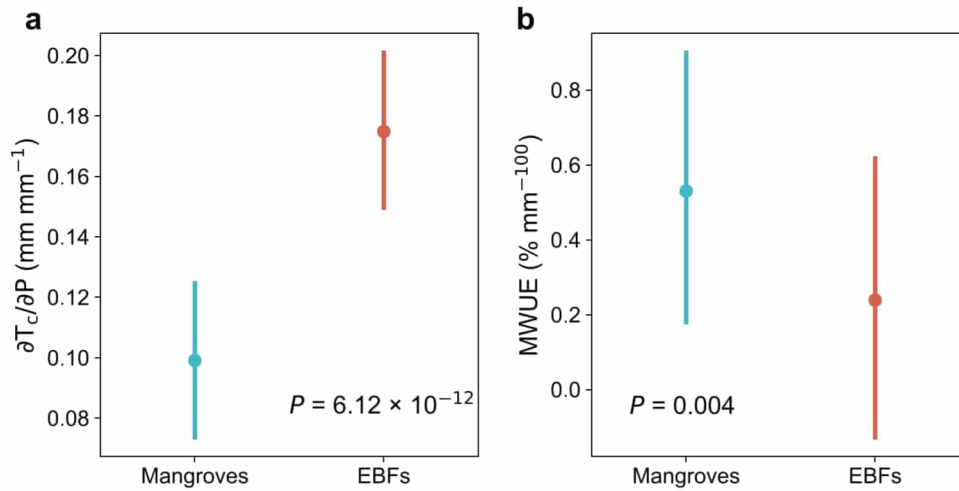


Extended Data Fig. 2 | Temporal variations in NIRv of mangroves and EBFs and environmental factors in coastal grids. a-e, Time variations in annual NIRv for mangroves and EBFs over the globe, America, Africa, Asia, and Oceania, respectively. NIRv are normalized by the long-term average. The dashed lines give the overall linear trend. The trend rates in the legend were computed from the Theil-Sen slope estimator. *P* values were determined through two-sided Mann-Kendall trend test. Shading indicates the 95% confidence intervals estimated

by bootstrapping ($n = 1000$). **f-j**, Interannual fluctuations in annual detrended NIRv for mangroves and EBFs over the globe, America, Africa, Asia, and Oceania, respectively. The numbers in the legend indicate the coefficient of variation of each NIRv time series to reflect the interannual variability. **k-o**, Time variations in annual temperature, precipitation and sea-level anomaly for the coastal grids over the globe, America, Africa, Asia, and Oceania, respectively.

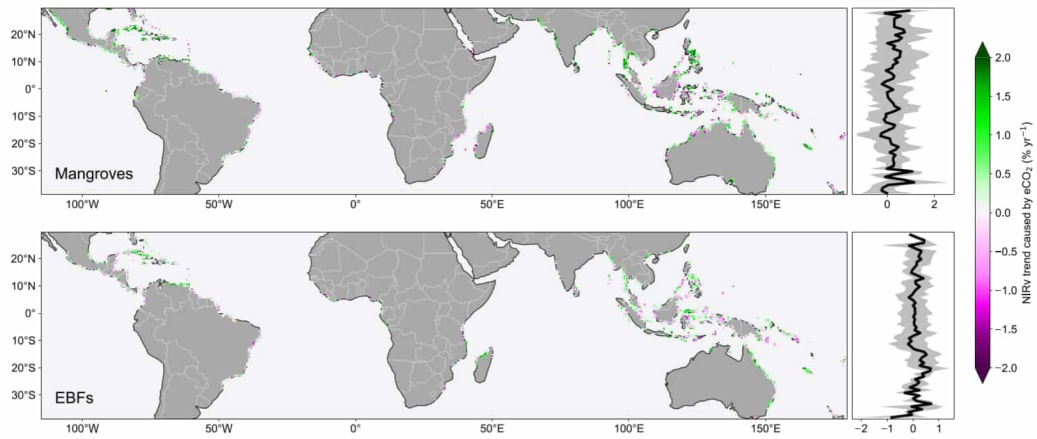


Extended Data Fig. 3 | Time series of annual NIRv (a) and environmental factors (air temperature, precipitation, and sea-level anomaly) (b) in the Gulf of Carpentaria, Australia. Temperature, precipitation and sea-level anomaly is from MERRA2, GPCP, and CMEMS datasets, respectively. Shaded areas show ± 1 standard deviation of the mean.

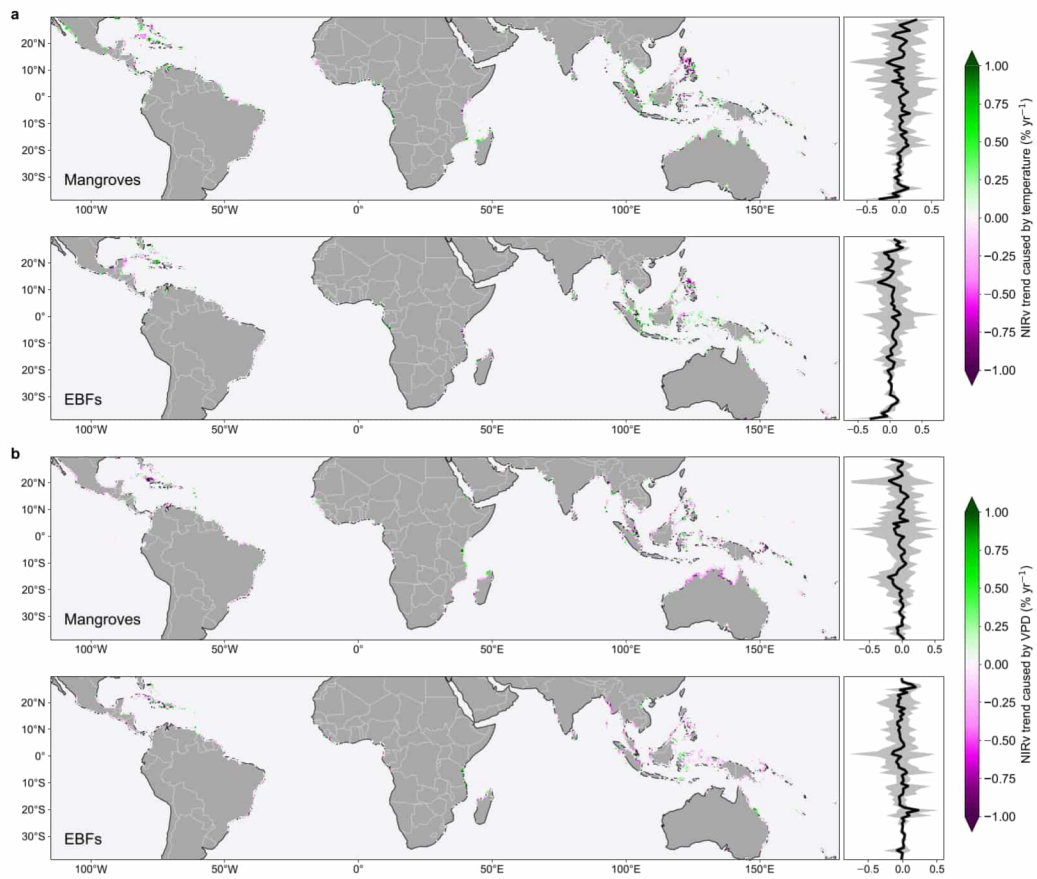


Extended Data Fig. 4 | The comparisons between mangroves and EBFs in their ecohydrological properties. Differences in marginal biological water use fraction ($\partial T_c / \partial P$) (a) and marginal water use efficiency (MWUE) (b). All comparisons were performed under controlled geographical conditions using

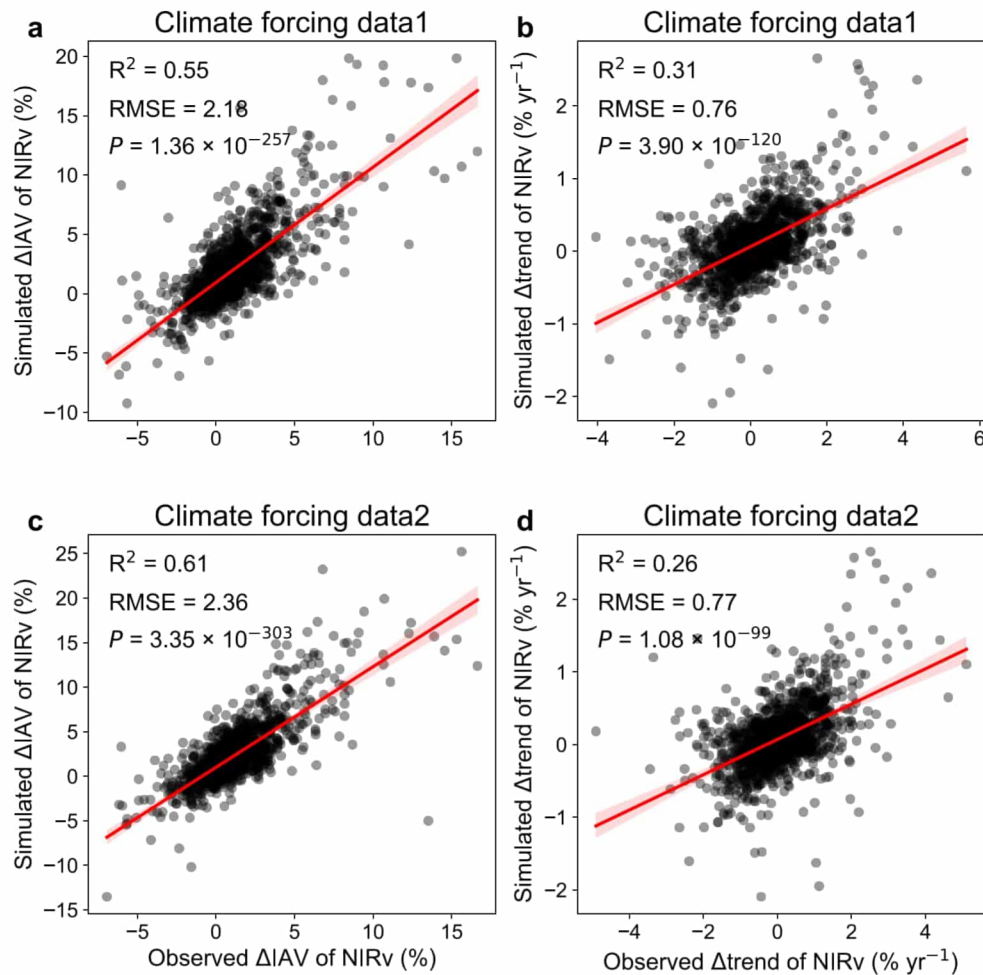
the two-sided paired *t*-test to eliminate spatial mismatch. Error bars show 95% confidence intervals estimated by bootstrapping ($n = 1000$), and the dots represent the average values.



Extended Data Fig. 5 | eCO₂-induced NIRv trends calculated using factorial simulation. The right panels depict the latitudinal pattern of trends averaged per 1° latitude band.



Extended Data Fig. 6 | Simulated NIRv trends for mangroves and EBFs, respectively. a, Temperature-contributed NIRv trends. b, VPD-contributed NIRv trends. The right panels depict the latitudinal pattern of trends averaged per 1° latitude band.



Extended Data Fig. 7 | Model performance in simulating observed difference in NIRv IAV and trend between mangroves and EBFs. **a,c.** Comparison of Δ IAV between observed and simulated from climate forcing data 1 (**a**) and climate forcing data 2 (**c**). **b,d.** Comparison of Δ trend between observed and simulated from climate forcing data 1 (**b**) and climate forcing data 2 (**d**). Climate forcing

data 1 represents factors from MERRA2, GPCP, and NOAA CarbonTracker CT2022 datasets. Climate forcing data 2 represents factors from ERA5, CHIRPS, TerraClimate and Mauna Loa observatory. Scatter refers to each paired coastal grid cell ($n = 1475$). The red shaded areas show 95% confidence intervals for the regression fits. P values were determined through one-sided F-test.

Reporting Summary

Nature Portfolio wishes to improve the reproducibility of the work that we publish. This form provides structure for consistency and transparency in reporting. For further information on Nature Portfolio policies, see our [Editorial Policies](#) and the [Editorial Policy Checklist](#).

Statistics

For all statistical analyses, confirm that the following items are present in the figure legend, table legend, main text, or Methods section.

n/a Confirmed

- The exact sample size (n) for each experimental group/condition, given as a discrete number and unit of measurement
- A statement on whether measurements were taken from distinct samples or whether the same sample was measured repeatedly
- The statistical test(s) used AND whether they are one- or two-sided
Only common tests should be described solely by name; describe more complex techniques in the Methods section.
- A description of all covariates tested
- A description of any assumptions or corrections, such as tests of normality and adjustment for multiple comparisons
- A full description of the statistical parameters including central tendency (e.g. means) or other basic estimates (e.g. regression coefficient) AND variation (e.g. standard deviation) or associated estimates of uncertainty (e.g. confidence intervals)
- For null hypothesis testing, the test statistic (e.g. F , t , r) with confidence intervals, effect sizes, degrees of freedom and P value noted
Give P values as exact values whenever suitable.
- For Bayesian analysis, information on the choice of priors and Markov chain Monte Carlo settings
- For hierarchical and complex designs, identification of the appropriate level for tests and full reporting of outcomes
- Estimates of effect sizes (e.g. Cohen's d , Pearson's r), indicating how they were calculated

Our web collection on [statistics for biologists](#) contains articles on many of the points above.

Software and code

Policy information about [availability of computer code](#)

Data collection ECOSTRESS transpiration data was downloaded from the original source. MODIS NIRv data and land-cover data used in this study were preprocessed and exported from Google Earth Engine.

Data analysis The code to estimate NIRv trends and IAV and the climatic sensitivities of mangroves and their adjacent terrestrial forests is available at <https://github.com/GIS-ZhangZhen/MangroveGreenness>.

For manuscripts utilizing custom algorithms or software that are central to the research but not yet described in published literature, software must be made available to editors and reviewers. We strongly encourage code deposition in a community repository (e.g. GitHub). See the Nature Portfolio [guidelines for submitting code & software](#) for further information.

Data

Policy information about [availability of data](#)

All manuscripts must include a [data availability statement](#). This statement should provide the following information, where applicable:

- Accession codes, unique identifiers, or web links for publicly available datasets
- A description of any restrictions on data availability
- For clinical datasets or third party data, please ensure that the statement adheres to our [policy](#)

All data used in this study are publicly available. The MODIS 250-m spectral reflectance data (MOD13Q1 and MYD13Q1) are available at https://developers.google.com/earth-engine/datasets/catalog/MODIS_006_MOD13Q1 and <https://developers.google.com/earth-engine/datasets/catalog/>

MODIS_006_MYD13Q1. Gridded climate data used in this study are available in the Supplementary Table 2. Forest cover data can be found at the following websites: Global Mangrove Watch v3.0 (<https://zenodo.org/record/6894273>), MCD12Q1 land-cover product (https://developers.google.com/earth-engine/datasets/catalog/MODIS_006_MCD12Q1), and global forest change map (https://developers.google.com/earth-engine/datasets/catalog/UMD_hansen_global_forest_change_2021_v1_9). ECOSTRESS ET data could be accessed at <https://www.jpl.nasa.gov/missions/ecosystem-spaceborne-thermal-radiometer-experiment-on-space-station-ecostress>. Atmospheric CO₂ concentration recorded by the Mauna Loa observatory can be accessed at <https://gml.noaa.gov/ccgg/trends/data.html>. The GPP measurements in the three mangrove sites are available in the Supplementary Table 1.

Research involving human participants, their data, or biological material

Policy information about studies with [human participants or human data](#). See also policy information about [sex, gender \(identity/presentation\), and sexual orientation](#) and [race, ethnicity and racism](#).

Reporting on sex and gender

Use the terms *sex* (biological attribute) and *gender* (shaped by social and cultural circumstances) carefully in order to avoid confusing both terms. Indicate if findings apply to only one sex or gender; describe whether sex and gender were considered in study design; whether sex and/or gender was determined based on self-reporting or assigned and methods used. Provide in the source data disaggregated sex and gender data, where this information has been collected, and if consent has been obtained for sharing of individual-level data; provide overall numbers in this Reporting Summary. Please state if this information has not been collected. Report sex- and gender-based analyses where performed, justify reasons for lack of sex- and gender-based analysis.

Reporting on race, ethnicity, or other socially relevant groupings

Please specify the socially constructed or socially relevant categorization variable(s) used in your manuscript and explain why they were used. Please note that such variables should not be used as proxies for other socially constructed/relevant variables (for example, race or ethnicity should not be used as a proxy for socioeconomic status). Provide clear definitions of the relevant terms used, how they were provided (by the participants/respondents, the researchers, or third parties), and the method(s) used to classify people into the different categories (e.g. self-report, census or administrative data, social media data, etc.) Please provide details about how you controlled for confounding variables in your analyses.

Population characteristics

Describe the covariate-relevant population characteristics of the human research participants (e.g. age, genotypic information, past and current diagnosis and treatment categories). If you filled out the behavioural & social sciences study design questions and have nothing to add here, write "See above."

Recruitment

Describe how participants were recruited. Outline any potential self-selection bias or other biases that may be present and how these are likely to impact results.

Ethics oversight

Identify the organization(s) that approved the study protocol.

Note that full information on the approval of the study protocol must also be provided in the manuscript.

Field-specific reporting

Please select the one below that is the best fit for your research. If you are not sure, read the appropriate sections before making your selection.

Life sciences Behavioural & social sciences Ecological, evolutionary & environmental sciences

For a reference copy of the document with all sections, see [nature.com/documents/nr-reporting-summary-flat.pdf](https://www.nature.com/documents/nr-reporting-summary-flat.pdf)

Ecological, evolutionary & environmental sciences study design

All studies must disclose on these points even when the disclosure is negative.

Study description

we examined the trend and inter-annual variability in productivity of global mangroves by using 20-years MODIS vegetation index measurements and further quantified their sensitivities to temperature, precipitation, sea level, wind, vapor pressure deficit, and CO₂ concentration and their unique characteristics compared to the adjacent terrestrial forests.

Research sample

We used 30-m resolution mangrove map from Global Mangrove Watch. All pixels mainly occupied by mangroves were used. We did not perform any post collection sampling.

Sampling strategy

No sampling strategy was used.

Data collection

The data used in this study are available in public repositories. Links to these repositories are provided in the manuscript.

Timing and spatial scale

We used global MODIS NIRv data and climatic datasets within mangrove areas from 2001 to 2020.

Data exclusions

Pixels having land-cover change between 2001 and 2020 were excluded to excluding impacts from direct interfere of human activities and sea-level rise and to separating the responses to climate change.

Reproducibility

Statistical analysis was fully reproduced when all data is analysed, as in this study.

Randomization

MODIS 250-m pixels were allocated as mangroves or terrestrial evergreen broadleaf forest according to the corresponding proportion. For instance, a MODIS 250-m pixel was classified as mangroves if its mangrove proportion is greater than 80%.

Blinding

Blinding is not relevant to this study as we do not compare control and treatment groups.

Did the study involve field work?

Yes

No

Reporting for specific materials, systems and methods

We require information from authors about some types of materials, experimental systems and methods used in many studies. Here, indicate whether each material, system or method listed is relevant to your study. If you are not sure if a list item applies to your research, read the appropriate section before selecting a response.

Materials & experimental systems

- | n/a | Included in the study |
|-------------------------------------|--|
| <input checked="" type="checkbox"/> | <input type="checkbox"/> Antibodies |
| <input checked="" type="checkbox"/> | <input type="checkbox"/> Eukaryotic cell lines |
| <input checked="" type="checkbox"/> | <input type="checkbox"/> Palaeontology and archaeology |
| <input checked="" type="checkbox"/> | <input type="checkbox"/> Animals and other organisms |
| <input checked="" type="checkbox"/> | <input type="checkbox"/> Clinical data |
| <input checked="" type="checkbox"/> | <input type="checkbox"/> Dual use research of concern |
| <input checked="" type="checkbox"/> | <input type="checkbox"/> Plants |

Methods

- | n/a | Included in the study |
|-------------------------------------|---|
| <input checked="" type="checkbox"/> | <input type="checkbox"/> ChIP-seq |
| <input checked="" type="checkbox"/> | <input type="checkbox"/> Flow cytometry |
| <input checked="" type="checkbox"/> | <input type="checkbox"/> MRI-based neuroimaging |